COMPOSITE SCAFFOLDS OF NATURAL AND SYNTHETIC POLYMERS FOR BLADDER TISSUE ENGINEERING

By

BENJAMIN J. LAWRENCE

Bachelor of Science

Oklahoma State University

Stillwater, Oklahoma

2004

Submitted to the Faculty of the
Graduate College of the
Oklahoma State University
in partial fulfillment of
the requirements for
the Degree of
MASTER OF SCIENCE
July 2006

COMPOSITE SCAFFOLDS OF NATURAL AND

SYNTHETIC POLYMERS FOR

BLADDER TISSUE

ENGINEERING

Thesis Approved

Dr. Sundararajan V. Madihally
Thesis Advisor

Dr. A.J. Johannes

Dr. R Russell Rhinehart

Dr. Karen A. High

Dr. A. Gordon Emslie
Dean of the Graduate College

Table of Contents

List of Tables

List of Figures

I. Introduction and Review of Relevant Literature

Over 400 million people worldwide suffer from bladder diseases[1]. Bladders are ravaged by cancer, birth defects, nerve damage, or trauma. When conservative therapies are ineffective, bladder augmentation or urinary diversion are recommended as alternative therapies [2]. In worst cases, patients can require extensive surgery or bladder transplants. Today, enterocystoplasty is the most utilized method for bladder augmentation using ileum, colon, or stomach segments [3]. In this technique a section of the patient's own stomach or intestine is used to patch the bladder wall This technique can lead to malnutrition, electrolyte alterations, peritoneal adherences, abscesses, enteric fistulae, excessive mucus production, bacterial colonization, and cancer [4]. In addition to the shortage of available organ and tissue donors there are other disadvantages associated with autografts, tissues taken from the patient, include complications such as the formation of bladder stones. The risk of complications rises when using allografts, tissues taken from human donors. Additionally, there is a risk of hyperacute rejection due to potential mismatch of xenografts, tissues taken from an animal source. These obstacles show the need for alternative repair options. Tissue engineering has been used in order to minimize these complications, and a variety of natural or synthetic materials have been used as alternative means of bladder augmentation [5]

Tissue Engineering

The basic approach of tissue engineering uses biodegradable scaffolds to support and guide the in-growth of cells (**Figure 1**.) Tissue scaffolds must be biodegradable, bioresorbable, biocompatible, and sterilizable. The scaffold must provide enough mechanical strength to withstand physiological stresses, must provide an environment suitable for cellular growth, and should contain suitable surface properties (wettability, stiffness, and compliance) to support cell attachment, proliferation, and differentiation. Eventually, the scaffold material disappears leaving only normal healthy tissue[6-8]. Additionally, the degradation products should be biocompatible, non-toxic, and transportable out of the body.

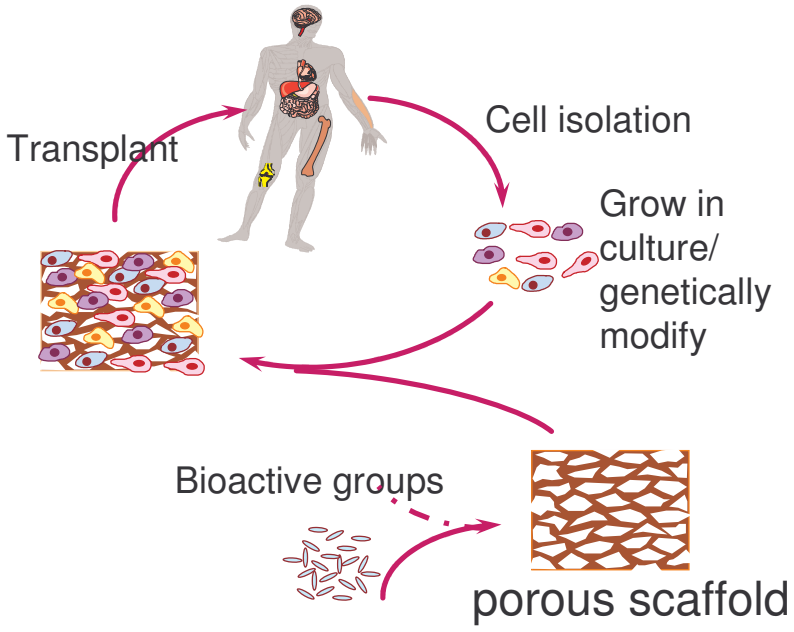

Figure 1. Concept of Tissue Engineering

Currently, there are two tissue engineering methodologies, "unseeded" and "seeded". The unseeded techniques involve the direct *in vivo* implantation of a biodegradable scaffold into the host bladder, allowing the natural process of regeneration to occur. In contrast, seeded techniques utilize *in vitro* cell culture of primary bladder cells, derived from host's tissue, on biodegradable scaffolds to establish cell-composite grafts, followed by *in vivo* implantation of the grafts. Scaffolds generated from natural polymers [9], synthetic polymers, or by removing the cellular components from xenogeneic tissues [1] have been used with and without prior cell-seeding to support and guide the in-growth of cells.

Natural Matrices

One option for creating tissue scaffolds is to use extracellular matrix (ECM) components derived from animal sources. For example porcine acellular dermis has been used for skin regeneration[10] and control of hypertrophic scarring [11]. Small intestinal submucosa (SIS) i another material that has shown significant success in various tissue engineering applications[12]. SIS is a dense connective tissue harvested from the small intestine. SIS is obtained after removing the mucosa, serosa, and muscle layers from the harvested tissue **(Figure 2**).

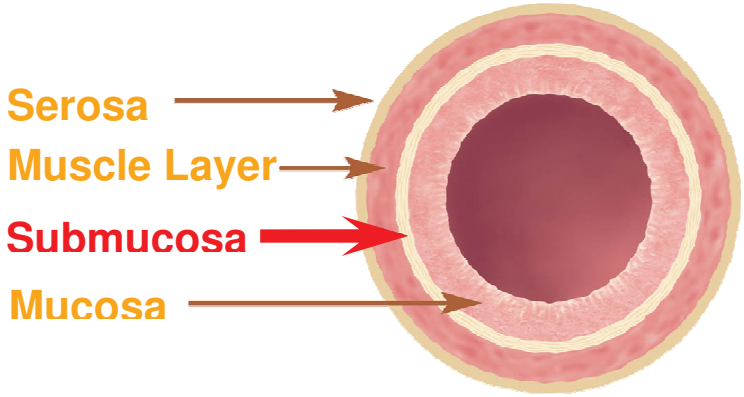

Figure 2. Layers within the Small Intestine

Porcine SIS has generated immense interest in various tissue engineering applications due to its diverse favorable properties [13,14]. SIS is the only bio-material that does not require cell seeding prior to in vivo implantation for bladder regeneration. SIS is rich in type 1 collagen, biocompatible, pliable, and resistant to infection. Additionally, SIS has a resorption rate of 4-16 weeks [15,16] and its immune response shows a phenotypic characteristic of tissue remodeling rather than rejection [17]. SIS promotes cell migration of numerous cell types and has been tested for regeneration of diverse tissues including large vascular grafts [18], venous valves and leaflets [19-21], skin [22], tendons [23], and wound dressing [24]. For urinary tract reconstruction, SIS has been used for bladder augmentation [25-27], for ureter [28] and urethra [25,29] replacement, and to promote regeneration of transitional epithelium, smooth muscle, and peripheral nerves with no evidence of immunological rejection [30]. Long-term studies show that SIS grafts can be remolded and replaced by the host and such regenerated tissues become histologically indistinguishable from native tissues [26]. The remodeled tissue shows complete regeneration of all three layers (mucosa, smooth muscle, and serosa) of the bladder in rat [31] and dog [32,33] models with only problem being low quality and disorganized smooth muscle fibers.

Additionally, SIS is commercially from a number of sources. COOK Biotechnlogy (West Lafayette, IN) sells single ply porcine SIS under the trade name Surgisis® at a cost of $286 per 7 cm x 10 cm sample[34]. COOK also sells multiply Surgisis® SIS, but multiply SIS does not provide reliable bladder regeneration compared to single ply SIS[35].

Large-scale preparation of SIS is hindered by various physiochemical properties which affect the quality and reliability of the tissue regeneration in clinical settings. The physical and mechanical characteristics of the matrix, such as permeability, thickness, tensile properties, fatigue properties, and ultrastructural properties, vary depending on the age of the animal, the sterilization technique, and the location within the small intestine it is harvested from [36].

Relative to home-made proximal SIS and COOK SIS, home-made distal SIS has the lowest permeability. COOK SIS (single ply) has the lowest tensile load bearing capacity relative to distal and proximal SIS. E-beam sterilization resulted in severe contraction and bone formation within the graft which was not observed after ethylene oxide sterilization[35]. Nevertheless, in a canine model study, bladder augmentation with distal SIS showed remarkably enhanced bladder regeneration relative to proximal SIS [37]. Further, SIS obtained from the distal region (**Figure 3**) of the intestine enables better cellular ingrowth and tissue remodeling than SIS taken from the proximal region [35]. Thus, forming synthetic matrices with physiochemical properties similar to distal SIS will be useful in bladder and other soft tissue regeneration.

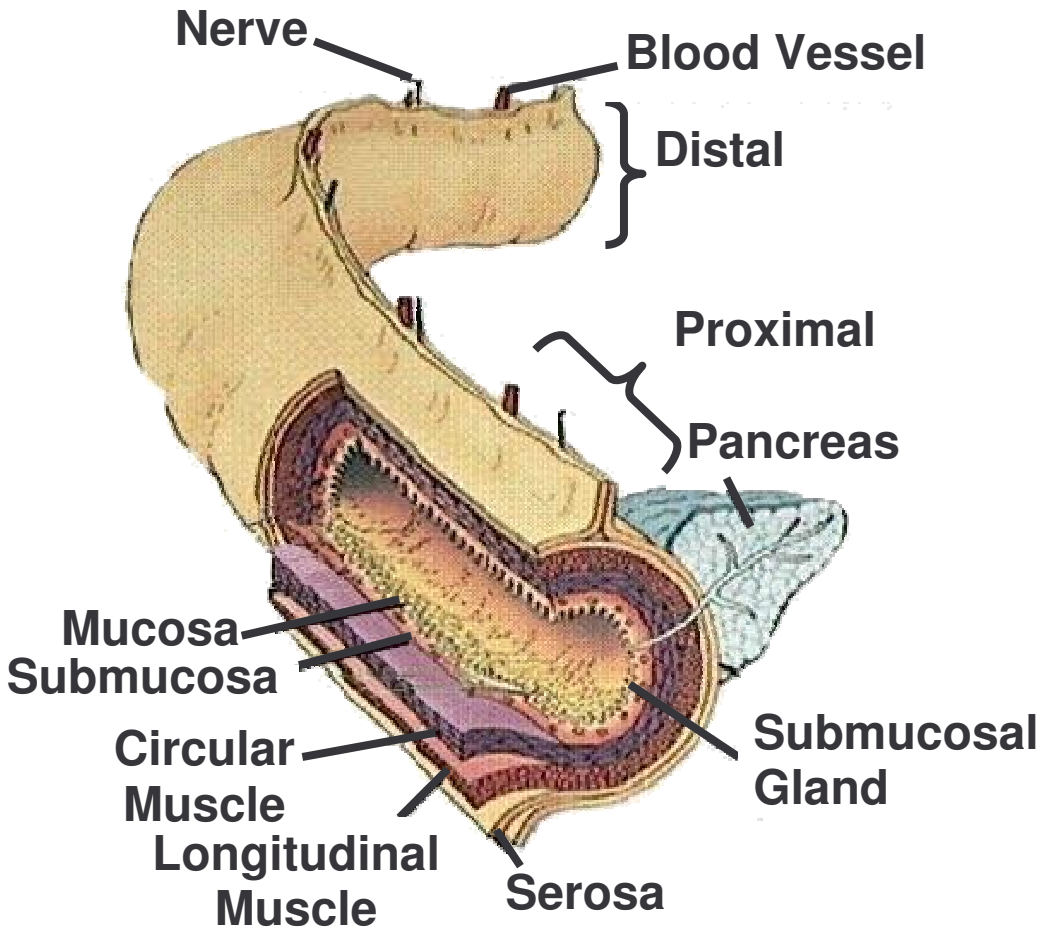

Figure 3. Location of the Submucosa within the Small Intestine

Formation of Three Dimensional Polymer Scaffolds

An alterative to using natural matrices is to synthesize polymer matrices for use as tissue engineering scaffolds. Both natural and synthetic polymers have been used in tissue engineering applications. It is also important to include a three dimensional porous structure into the scaffolds to promote cellular ingrowth and differentiation [38].

Several techniques have been developed to fabricate porous scaffolds, including solvent casting/particulate leaching [39], fiber bonding (unwoven meshes) [40], gas foaming [41], and phase separation/emulsification [42]. Another method to fabricate porous scaffolds is

to introduce a porogen such as salt (NaCl) into the polymer and then remove it with a solvent (particulate leaching) [43]. The leaching of salt from a polymer composite can form pores within scaffolds, the pore sizes are dependent on the size and amount of salt crystals. Pore size and distribution is difficult to control. Gas porogen has been used as alternative to eliminate the use of organic solvents (gas foaming). But the pores created in this method are non-uniform, limiting cell seeding and migration [40].

Scaffolds can be formed using 3D printing techniques. Scaffolds are built layer by layer, and the pore size and spacing are controlled by the pattern used. The advantage to 3D printing is the control of pore size and distribution. The disadvantage is that the fiber diameter limits the pore sizes and configurations possible. Currently, construction is limited to a 150 μm fiber diameter [44]. Direct writing processes are also limited by the ink used. To assure successful printing the ink must be viscous enough to holds its shape after printing but not so viscous that it is too difficult to pump. Additionally the ink must quickly form the polymer fiber after printing, as well as bond to previously printed layers.

3D porous scaffolds can also be created using standard microfabrication techniques including microembossing[45] and soft lithography[46,47]. Microfabricated scaffolds can be produced that contain both pores and nano-scale surface features, enabling better control of the cellular microenvironment.

Scaffolds with nanofibers can be produced using electrospinning process[48,49,50]. In the process of electrospinning a non-woven matrix is formed by directing a charged polymer solution at an oppositely charged collector. Additionally, changing the orientation of the collector can produce both random and aligned nanofibers arrangements.

Three dimensional scaffolds can also be formed using hydrogels, water soluble polymers crosslinked into a 3D matrix[51]. One of the prime advantages to hydrogels is that they can be polymerized *in situ* by thermo-gelling[52] or photocrosslinking [53,54]. Another advantage is that cells can be encapsulated directly into the scaffold, providing faster tissue ingrowth. In autoimmune disorders, like diabetes, hydrogels can serve as a protective barrier between the implanted functional cells and the immune system [55].

Due to a number of advantages this study used controlled rate freezing and lyophilization to create the porous chitosan structures [56]. By controlling the rate of freezing, ice crystals form in the solution following the path of heat flow. While the solution freezes the polymer precipitates out of solution and is trapped between the ice crystals. The solvent is then removed by freeze drying, leaving the porous polymer structure intact. The pore size is determined by the size of the ice crystals. Therefore, the size and orientation of pores can be directed by controlling the rate and direction of freezing. By freezing at a constant temperature the pore size becomes a function of freezer temperature; quicker freezing will produce smaller pores. This process also avoids heat denaturation of biological materials because it is performed at low temperature. This allows bioactive molecules to be included in the scaffold without altering their activity, if necessary.

Importance of 3D Architecture

Recent advances in tissue culture have shown that cells respond differently in attachment, morphology, migration and proliferation on a 3D scaffold then in traditional two-dimensional tissue culture[38]. Many cell types such as fibroblasts, mesenchymal stem cells, epithelial cells, and neural crest cells show different adhesions when grown on 3D matrices as opposed to 2D cell culture [57,58]. In 2D substrata, cultured cells are restricted to spreading and attaching to a flat rigid glass or tissue culture plastic surface coated with different substrates. The influence of biophysical properties of the material may be overwhelmed by the effect of the rigid surface. However, biophysical properties significantly influence cell adhesion, signaling and functions in 3D environment. Further, the 3D architecture could distribute binding sites differently than 2D architecture [57,59]. 3D focal adhesions appear distinct from 2D focal adhesions on a rigid 2D matrix and are termed as "3D matrix adhesions" to separate them from 2D counterparts. In addition to proteins present in focal adhesions on 2D matrices, cells may have cytoskeletal adaptor proteins on 3D matrix [57,60]. Such discrepancy in cell adhesion between 2D vs. 3D causes different signal transduction, subsequent altered cell morphology and rearrangement. In response to different physical and chemical signals from surrounding 3D matrix, cells can synthesize ECM components and the degradation of matrix can create spatial advantages for cell expansion and forward migration, unlike 2D architecture. Pore size and void fraction [61-65], stiffness, pore interconnectivity, and topography[66] can affect cell colonization in synthetic scaffolds. A majority of the cells are unable to completely colonize scaffolds with pore sizes > 300 nm due to difficulty in crossing large bridging

distances[61]. An optimum pore size range for many cell types is 100 – 150 nm. Hence matrices with that pore size range are preferred in many applications.

Synthetic Polyesters

Synthetic polyesters such as poly (lactic acid) (PLA), poly (glycolic acid) (PGA), their copolymers (PLGA, PLLA, etc) [67-73], and poly (caprolactone) (PCL) [74,75] have generated immense interest as tissue engineering materials due to their strong approval history (few products are FDA approved) and numerous investigations in a variety of biological applications for more than three decades [76]. These polymers degrade by hydrolysis (i.e., non-enzymatically). Their degradation rates and mechanical properties can be altered via co- and graft-polymerization techniques [77-79], and by processing conditions [80-83].

PGA is a rigid thermoplastic material with high crystallinity and is hydrophilic [84]. PLA is more hydrophobic than PGA due to an extra methyl group in the lactide molecule. Because lactic acid is a chiral molecule, PLA has D-PLA and L-PLA stereoisomeric forms. Of the two isomers L-PLA is more frequently used in tissue engineering because it possesses high mechanical strength [85]. Poly (lactic-co-glycolic acid) (PLGA) is the copolymer of glycolic acid and lactic acid (**Figure 4**). Various ratios (75 PLA:25 PGA, 50:50, etc) of PLGA have been investigated. Amorphous 50:50 PLGA (50% lactic acid, 50% glycolic acid) is preferred for various tissue engineering applications because it degrades faster than other co-polymer ratios, which are semi-crystalline. The degradation of PLGA is via random hydrolysis of the ester bonds. In addition, the degradation rate can be modified by changing the copolymer ratio and molecular weight (lower molecular weights degrade faster) [86].

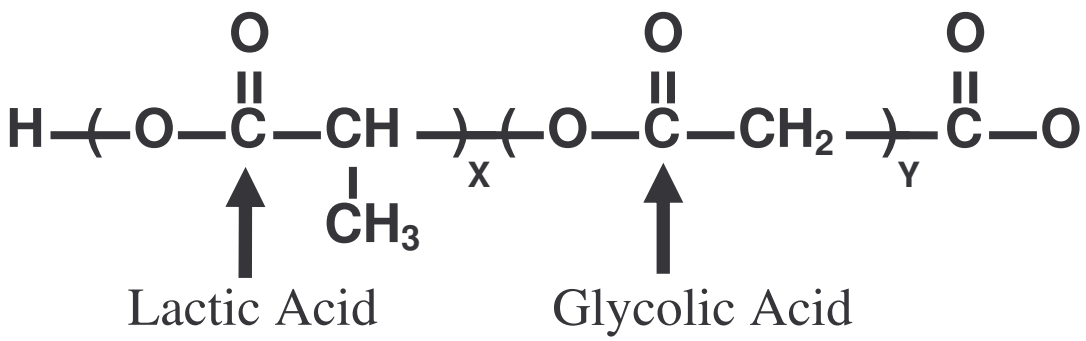

Figure 4. Chemical Structure of PLGA

Poly (caprolactone) (PCL) is a non-toxic, biocompatible aliphatic polyester [86]. PCL has a degradation time dependent on its molecular weight. High molecular weight degradation times are of the order of two to three years make which it unsuitable for short term implants [87]. The rate of degradation can be altered by copolymerization with other polymers.

Poly (propylene fumarate) (PPF) based polymers have been developed as injectable materials for orthopedic applications [86]. PPF can be photo cross-linked with poly (propylene fumarate)-diacrylate (PPF-DA) by free radical polymerization to form solid polymeric networks with high compressive strength at a bone fracture site[88]. The degradation of PPF produces fumaric acid and propylene glycol and the degradation time is dependent on the polymer structures.

Synthetic polymers show poor regulation of cellular activity [89]. Furthermore, their degradation products are relatively strong acids and cause inflammation [90]. The scaffolds also show structural instability due to massive swelling during degradation [82]. Apart from adhesive interactions, a substrate has to mediate a variety of signals such as growth factor activity to regulate the biological response of diverse cell types. Despite

significant efforts to improve these limitations via co-polymerization [91] and grafting arginine-glycine-aspartate (RGD) peptides (necessary for cellular attachment) [92], recreating all the biological responses may be beyond current capabilities.

Natural Polymers

Natural polymers are derived from a variety of sources including fish scales, rat tails, and crab shells. Unlike synthetic polymers, natural polymers have superior biological properties. However, natural polymers lack physical strength. Porous scaffolds formed of natural polymers have a modulus of only 2 kPa, compared to 3 MPa for SIS.

Chitosan is a polysaccharide derived from N-deacetylation of chitin, a polymer present in the outer shells of crustaceans. Chitosan is composed of β (1-4) linked 2-acetamido-2-deoxy-D-glucose and 2-amino-2-deoxy-D-glucose units (**Figure 5**). It is a semi-crystalline polymer, and the crystallinity is dependent on the degree of deacetylation. Chitosan is structurally analogous to glycosaminoglycan (GAG), an extra cellular matrix (ECM) element present in the human body. Since GAG has specific interactions with growth factors/proteins, chitosan may share similar activity. Chitosan is insoluble in water or organic solvents but soluble in aqueous acids (pH< 6.3). Due to the protonation of the free amine groups on the chain backbone (**Figure 5**), chitosan exhibits a high charge density in solution. This cationic nature and high charge density allow favorable interactions with negatively charged cells as well as antibacterial activity. Chitosan has been widely investigated in wound dressing and drug delivery systems [93]. The biocompatibility and biodegradability of chitosan makes it a promising material for tissue engineering[94]. Chitosan has shown biological activity towards diverse cell types

including stem cells[95,96], chondrocytes[96,97], osteoblasts[97], hepatocytes[78,98], and Schwann cells [99,100]. In addition, chitosan has minimal immune reaction and its stimulatory effect can induce local cell proliferation[95]. Chitosan can be degraded by lysozyme, a naturally occurring enzyme *in vivo*[56]. The biodegradation time is determined by the amount of residual acetyl content, an easily controlled variable. Due to the active amino groups (**Figure 5**), chemical modification of chitosan can produce materials with a variety of physical and mechanical properties. Polysaccharide scaffolds were synthesized by crosslinking arabinogalactan, dextran and amylose with chitosan to create a more cell compatible environment [101]. Chitosan is also blended with collagen, alginate, GAG, and synthetic polymers (i.e. PLGA, PCL) to fabricate suitable scaffolds [102]. The pH dependent solubility, the easy processability under mild conditions, the modification reactivity, the biodegradability, and biocompatibility make chitosan an excellent candidate for use as porous scaffolds in tissue engineering.

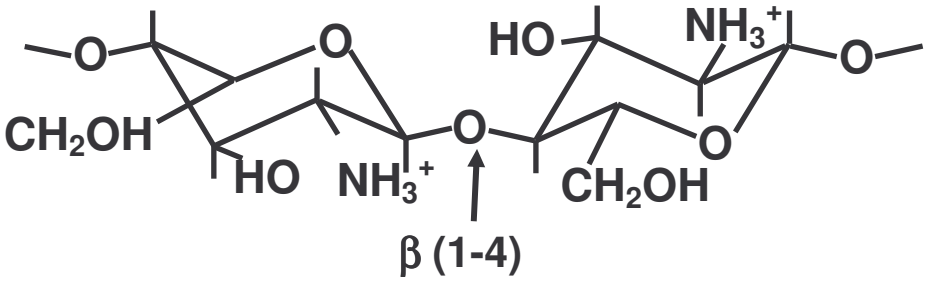

Figure 5. Chemical Structure of Chitosan

Hyaluronan, a large linear GAG, is composed of repeating disaccharide of D-N-acetylglucos-amine-β-D-Glucuronic acid [103]. It is negatively charged, acts as a polyelectrolyte in solution, and acts as a lubricant [104]. Although hyaluronan is involved in mediating cell adhesion as an ECM component, its degradation rate is difficult to control [84].

Collagens are a family of structural proteins reinforcing a variety of animal tissues including skin, bone, and tendon. Type I collagen is a major component of most connective tissues and present in the arterial wall [85] and may be degraded by several matrix metalloprotenases (MMPs) [105]. Collagen contains cellular-binding domains and has been extensively used in vascular tissue engineering.

Gelatin, a partially denatured derivative of collagen, has also been used to generate scaffolds. Gelatin is widely found in nature, and can be extracted from collagen found in fish, bovine bone, and porcine skin. The physicochemical properties of gelatin can be suitably modulated due to the existence of many functional groups. Gelatin blended with chitosan has been used in artificial skin and cartilage applications due to the ability to form a polyelectrolyte complex [106,107].

Fibrin has been used for cartilage repair [108]. Upon injury, fibrinogen self-assembles to become 3D fibrin hydrogel [84]. Fibrin can bind to different integrin receptors to regulate cytokine gene expression as well as regulate inflammation. Since fibrinogen can be obtained from the patient's own blood, use of fibrin minimizes immunogenic concerns. Another advantage of fibrin is that it can be degraded by cell-associated enzymatic system. Despite these advantages, fibrin scaffolds failed to keep their shape integrity. Fibrin gels showed significant reduction in size after *in vitro* incubation and weak compression modulus [109], suggesting a need for further modifications.

Polyhydroxyalkanoates are polyesters produced in microorganisms. The molecular weight of these polymers can be tailored by varying bacterial strain and media composition [110]. Most of these homopolymers are highly crystalline, brittle and have a

very long degradation time (up to years). Thus they are not suitable for scaffolding materials unless blended with other materials compensating for the disadvantages.

Combining Natural and Synthetic Polymers

While natural materials have the benefits of facilitating cell adhesion and repopulation by providing critical signals, they lack tailorability of mechanical properties. In contrast, synthetic materials possess advantages of easy control of microstructure, strength and degradation rate, but they lack growth factors and other signals to direct cell growth, proliferation, and differentiation [85]. Previous research has shown that it is possible to combine natural and synthetic polymers. One method is to create an emulsification system[111]. The emulsification system was required because there is no universal solvent for both hydrophilic natural polymer and hydrophobic synthetic polymers, and therefore, the polymers could not simply be blended.

Scaffolds were synthesized from the emulsions of the chitosan-PLGA blends (**Figure 6A**)[111]. Cellular activity of enhanced green fluorescence protein (EGFP)-transfected primary bladder- smooth muscle cells (SMC) was tested on these scaffolds. These results showed minimal cell spreading and proliferation on the scaffolds (Error! Reference source not found.**B**). Recently, it was shown that the observed difference in these emulsions is due to structural weakness in the matrix and minimal electrostatic cell adhesion to chitosan[95]. However, **Figure 6C** shows that the acidic degradation products of PLGA significantly influenced the degradation kinetics of lysozyme-dependent chitosan degradation. Thus, the only benefit of the PLGA, chitosan emulsion was an increased degradation rate of chitosan. Another problem with the emulsified scaffolds

was their lack of physical strength. The emulsified scaffolds have a modulus of only 2 kPa, compared to 3 MPa for SIS.

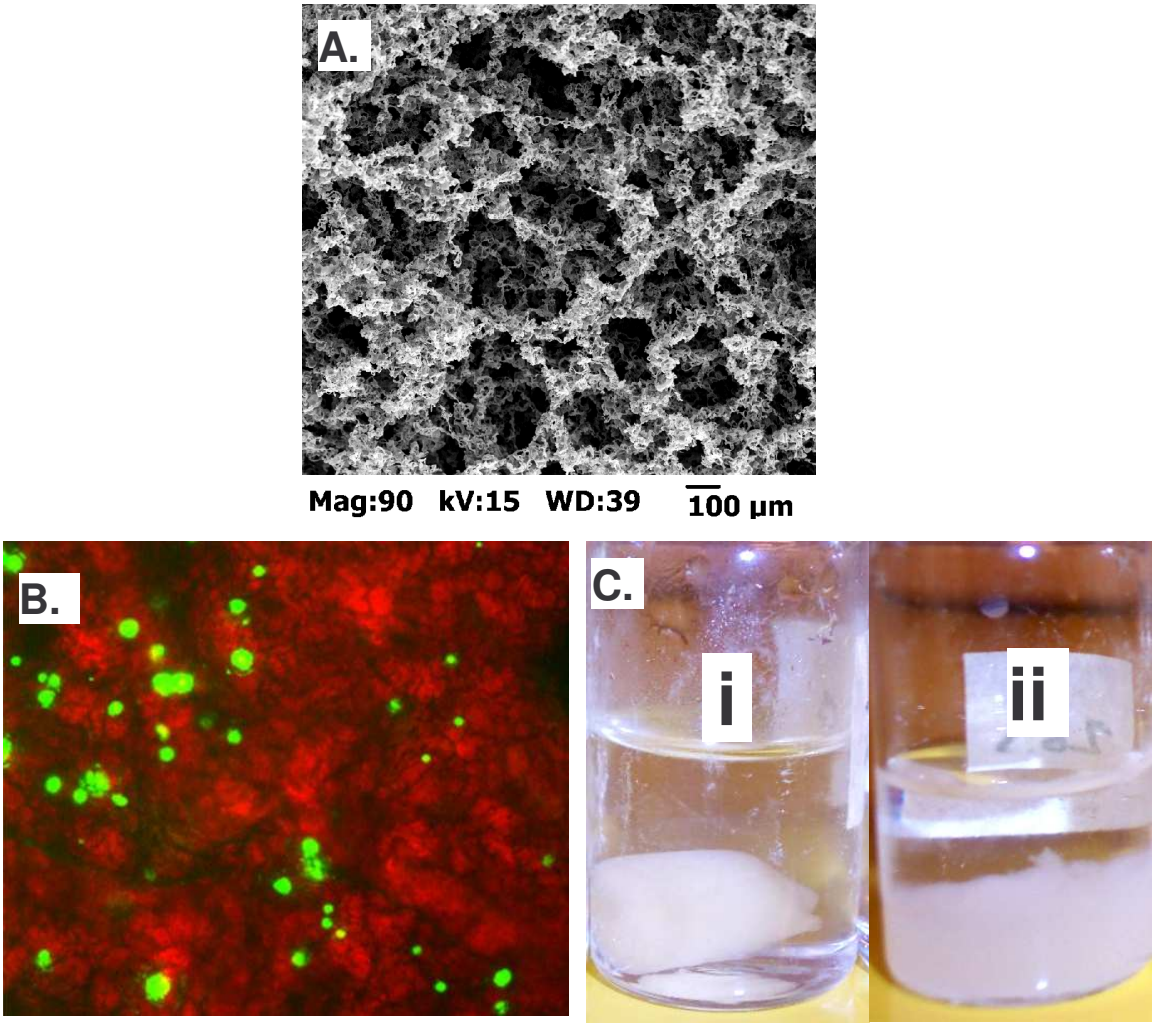

Figure 6. Emulsified Chitosan-PLGA Scaffolds

Panel A. 50:50 PLGA was blended with chitosan and matrices were formed using controlled rate freezing and lyophilization. Panel B. On to PLGA-chitosan matrix, GFP-transfected SMCs were seeded and micrographs were obtained after 4 days in culture. Panel C. Scaffolds were incubated in presence or absence of 10mg/L lysozyme. Photographs taken after 24 days i) chitosan in PBS, and ii) chitosan-PLGA in PBS containing lysozyme [111].

II. Hypothesis

An alternative to uniformly blending natural and synthetic polymers is to form composite matrices where the strengths of each polymer can be exploited while its weaknesses are minimized. Natural polymers (chitosan, gelatin, etc) have superior biological properties but degrade slowly and lack physical strength [95]. Synthetic polymers (PCL, PLA, PGA, PLGA, and others) have strength, elasticity, and tunable degradation properties but lack appropriate biological activity. A composite material formed by layering 3D porous chitosan and PLGA films may provide the individual advantages of the pure polymer membranes while overcoming the limitations inherent in the polymer type.

In one possible composite configuration, the outer chitosan layers provide biological activity while the PLGA layer provides mechanical strength. The difficulty inherent in creating a composite scaffold is attaching the hydrophobic PLGA layer to the hydrophilic chitosan layers. A possible method to ensure connection between the layers is to perforate the PLGA film and have the porous chitosan run continuously through the perforations. Hence, the main goal in this project is to develop a process to produce multi-layered composite scaffolds containing both natural and synthetic polymers.

Once the process is created the scaffolds should be characterized. Therefore, the tensile properties, permeability to urea, degradation behavior, and cell culture behavior of the composite scaffold will also be tested. The underlying goal is to produce a composite scaffold with physiochemical properties similar to distal SIS.

III. Materials and Methods

Sources for Material

PLGA (50:50, molecular weight = 160 kDa) was purchased from Birmingham Polymers (Birmingham, AL). Chitosan with >310 kDa MW and 85% degree of deacetylation, urea, Dulbecco's modified Eagle medium (DMEM), lysozyme, glucose, sodium bicarbonate, and resazurin were obtained from Sigma Aldrich Chemical Co (St. Louis, MO). A urea assay kit was obtained from Diagnostic Chemicals Limited (Oxford, CT). Mouse embryonic fibroblasts (referred to as STO cell line) were purchased from American Tissue Culture Collection (Walkersville, MD). L-glutamine, penicillin-streptomycin, amphotericin, trypsin/EDTA, and Fetal Bovine Serum (FBS) were purchased from Invitrogen Corp. (Carlsbad, CA).

Composite Layered Scaffold Fabrication

The composite structure is formed in layers as shown in **Figure 7**. First, a Teflon sheet is affixed to a flat aluminum plate using silicon glue. Teflon is used to provide a nonstick surface for the PLGA and the aluminum provides physical support to keep the Teflon flat. A 6 cm x 8 cm well is formed on the Teflon sheet using silicon glue (see **Figure 8A**). Five milliliters of 4% PLGA solution, prepared in chloroform, was poured into the well and air dried in a chemical hood overnight. The silicon is trimmed away and the PLGA film is perforated with a custom punching apparatus. The puncher consists of a Teflon grid marked in a 1 cm x 1 cm grid. The PLGA film is placed on the grid and perforations are made using stainless steel nails and a hammer (see **Figure 8B**).

At this point some samples were analyzed under a light microscope in order to measure the perforation size (as described in the thickness characterization section below). The perforated film is affixed to the Teflon sheet using silicon glue, forming another well. The well is filled with 10 mLs of 0.5% acidified chitosan solution, frozen at -80ºC, and lyophilized overnight. After the silicon is removed again, the sample is flipped, and a new well formed with silicon glue. Ten mL of chitosan solution is then added to the well, frozen at -80ºC and lyophilized overnight. The silicon is removed and the samples are stored in a vacuum desiccator. Before use, the composite membranes are neutralized in ethanol and washed with phosphate buffered saline (PBS).

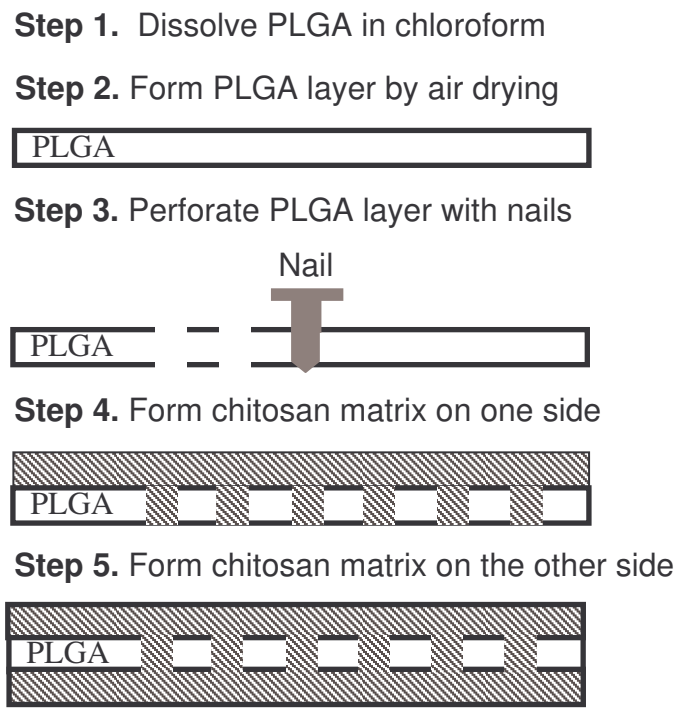

Figure 7. Formation of Composite Scaffold

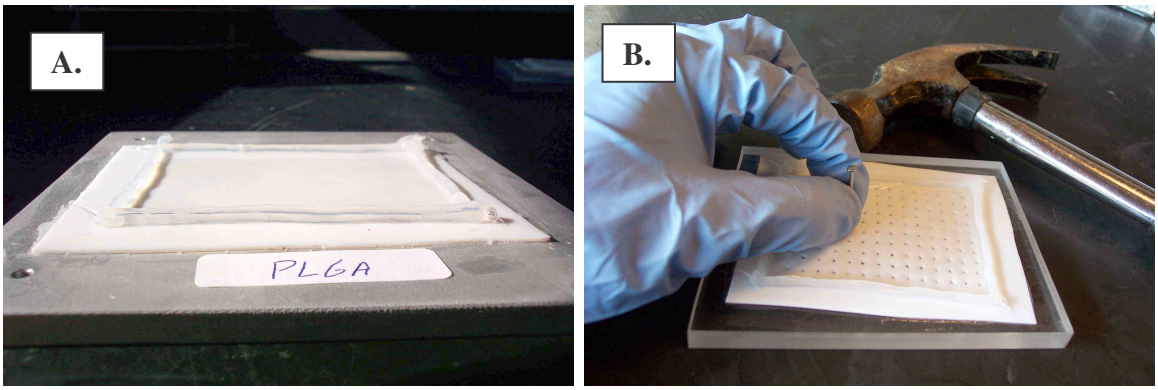

Figure 8. Construction of the Composite Scaffold

Panel A. Silicon glue is used to create a well for solvent casting. Panel B. The custom punching apparatus used to create perforations in the PLGA films

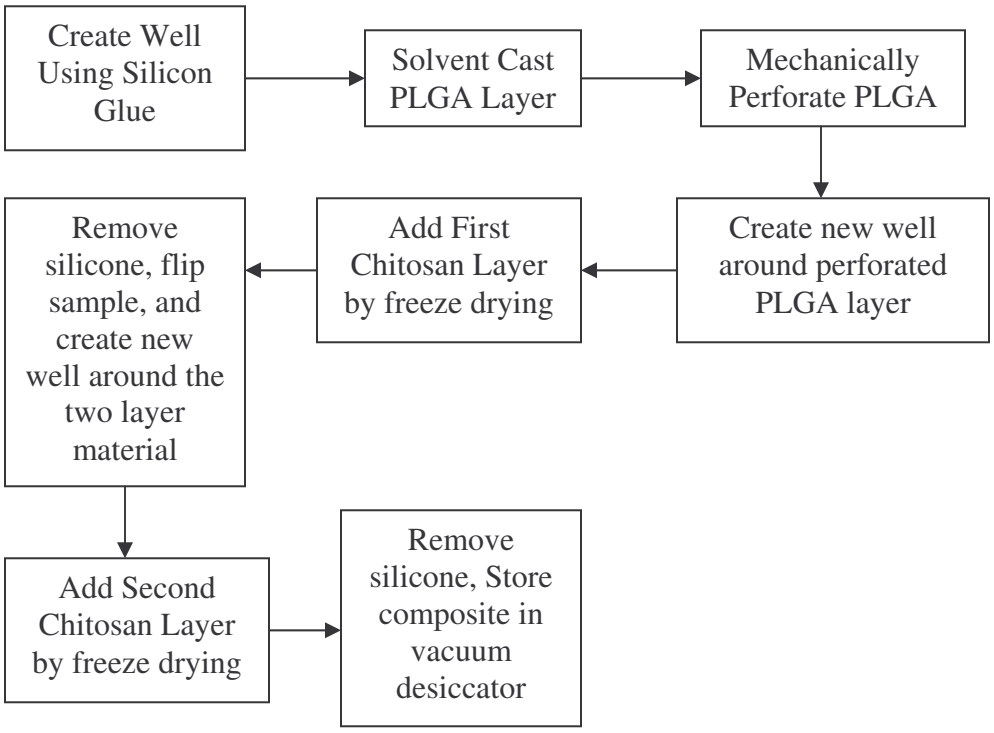

Figure 9. Flowchart of Process

Thickness Characterization

PLGA films were cast in Teflon wells as described, cut into small (2 mm) pieces, and oriented on a microscope slide so the cross section could be seen. An image of the cross section was recorded using an inverted microscope and digital camera. The cross section was then measured using Sigma Scan Pro software (Systat Software, Inc., Point Richmond, CA) which was calibrated using an image of a hemacytometer. See **Appendix 1** for more details.

Uniaxial Mechanical Testing

To measure tensile properties the composite membranes were cut into 6 cm x 1 cm strips and analyzed using an INSTRON 5842 (INSTRON Inc., Canton, MA) with a constant crosshead speed of 10 mm/min. Tensile tests were performed at room temperature under hydrated conditions using a custom designed chamber. See **Appendix 2** for more details.

Analysis of Microarchitecture

To evaluate the microarchitecture of the matrices, samples were analyzed using a scanning electron microscopy (SEM, Joel scanning microscope). For this purpose, samples were dehydrated using a series of increasing concentrations of ethanol followed by a brief vacuum drying. Samples were sputter coated with gold at 40 mA prior to observing under SEM. See **Appendix 3** for more details.

Measurement of Permeability

Permeability was measured using a modified version of the method developed by Raghavan et al [36]. This method utilizes a custom designed chamber shown in **Figure 10**. The chamber's diameter is 2 cm and each side has a holdup volume of 4 cm^3. The first chamber was filled with 550 mM urea in PBS. The 550 mM concentration corresponds

to the average physiological concentrations present in human urine[36]. A 2.5 cm x 2.5 cm section of the composite is placed on top of the solution, and the chamber is assembled. The other side of the sample (chamber 2) is filled with PBS using a syringe through the sample port. The chamber was maintained at room temperature. Small samples (100 μL) were taken at regular intervals beginning after the chamber was assembled and continuing for 8 hours. The concentration of urea was determined using a commercially available kit following the vendor's protocols (Diagnostic Chemicals Limited, Oxford, CT). In brief, 20 μL of sample was added to 2 mL of urease solution and the rate of change in absorption, at 340 nm, was measured for 90 s. The concentration of urea was determined using a calibration curve prepared between 0 to 275 mM urea.

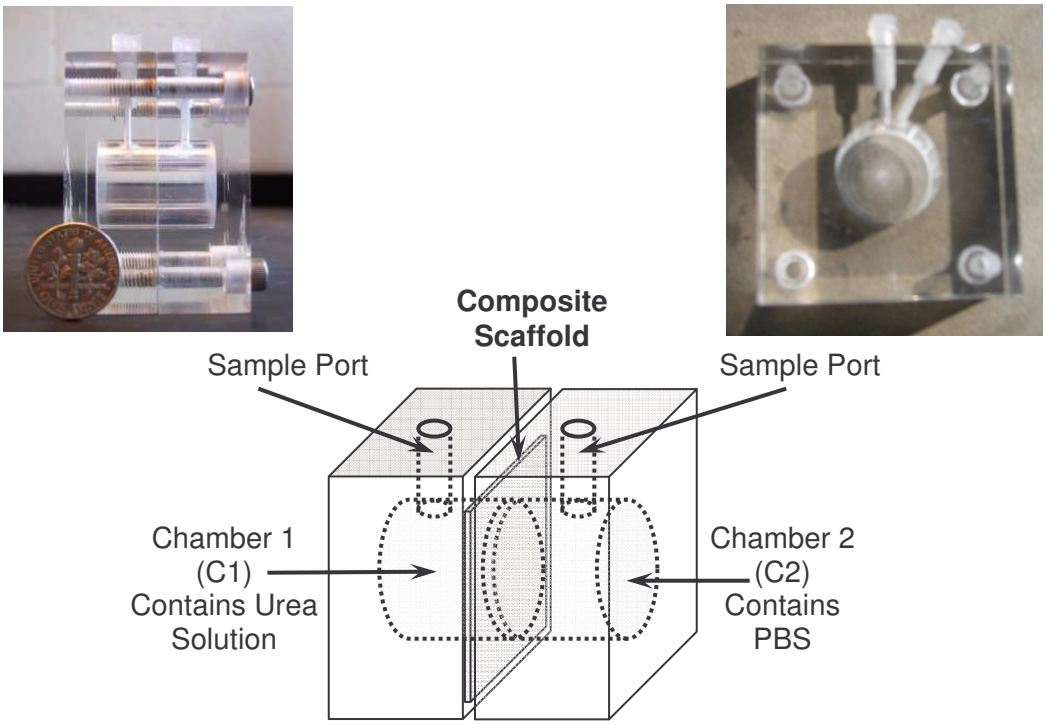

Figure 10. Diagram of the Chamber used in Permeability Experiments

Degradation Study

The degradation behavior of the composite scaffold was also examined. A degradation study was performed in standard 24-well cell culture plates using a modified procedure from Huang et al [95]. In brief, samples were cut into 1 cm x 1 cm pieces and placed into individual wells. The samples were washed with ethanol, rinsed twice with PBS, and incubated at 37ºC in PBS containing 10 mg/L lysozyme. The lysozyme containing PBS solution was changed every 7 days and the pH of the spent PBS was measured. Samples were removed at 1, 3, 8, 14, 21, and 28 days, dehydrated in a graduated series of ethanol washes (0, 25, 50, 80, 100%), and weighed. The samples were then examined by SEM to evaluate changes in the microarchitecture as described before.

Cell Culture

Mouse embryonic fibroblasts were grown in DMEM supplemented with 4 mM glutamine, 4.5 g/L glucose, 1.5 g/L sodium bicarbonate, 100 U/mL penicillin-streptomycin, 2.5 mg/mL amphotericin B, and 10% Fetal Bovine Serum (FBS). Cells were maintained at 37ºC, in a 5% CO_2/95% air and fed with fresh medium every 48 h. Cells were dissociated with 0.01% trypsin / 10 mM EDTA, centrifuged, and resuspended in medium prior to cell seeding.

PLGA films, with and without perforations, 3D chitosan matrices, and the trilayer composite were prepared as described previously. The samples were cut into 3 cm x 4 cm pieces and placed in sterile 6 well cell culture plates. The samples were sterilized by pure ethanol for 10 minutes and washed twice with PBS. The PBS was replaced with cell growth media and the samples were seeded with 200,000 cells/sample. The cells were allowed to grow for two days. The samples were then examined with a light microscope to determine attachment of seeded cells.

IV. Results

Composite Scaffold Physical Properties

One obstacle in fabricating the composite scaffolds was attaching the hydrophobic PLGA layer to the hydrophilic chitosan layer. The solution was to perforate the PLGA layer and have the chitosan compartment run continuously through the resultant holes. The scaffolds were analyzed with SEM at all points of construction to ensure the 3D structural design elements were incorporated into the final scaffold.

The PLGA perforations were rectangular with sides between 300 and 550μm long (**Figure 11A**). The perforation size is determined by the size of the nail used. When a single chitosan layer has been added the porous chitosan can be seen through a perforation in the PLGA layer (**Figure 11B).** This shows that there is good contact between the layers. After a second layer of porous chitosan is added, micrographs show that the chitosan forms a continuous layer through the perforations (**Figure 11C**). Micrographs of the composite structure show all three distinct compartments and that the chitosan remains porous on both sides (**Figure 11D**). The continuity of the chitosan is also supported by uneven areas on underside of composite membrane that follow the same pattern as the perforations. Additionally, the hydrated scaffold does not delaminate or come apart, further demonstrating that the composite is firmly anchored at the perforations. This data shows that the new fabrication process forms multi-layer composite scaffolds containing both natural and synthetic polymers.

The thickness of the composite scaffolds is roughly 2mm, much larger than SIS (thickness 200μm). Using the custom Teflon-silicon well plates PLGA membranes were obtained with a thickness of 50 ± 16μm. Therefore, large thickness is a result of the surface tension and viscosity of the chitosan solution. The chitosan solution has limited spreading on the hydrophobic PLGA film.

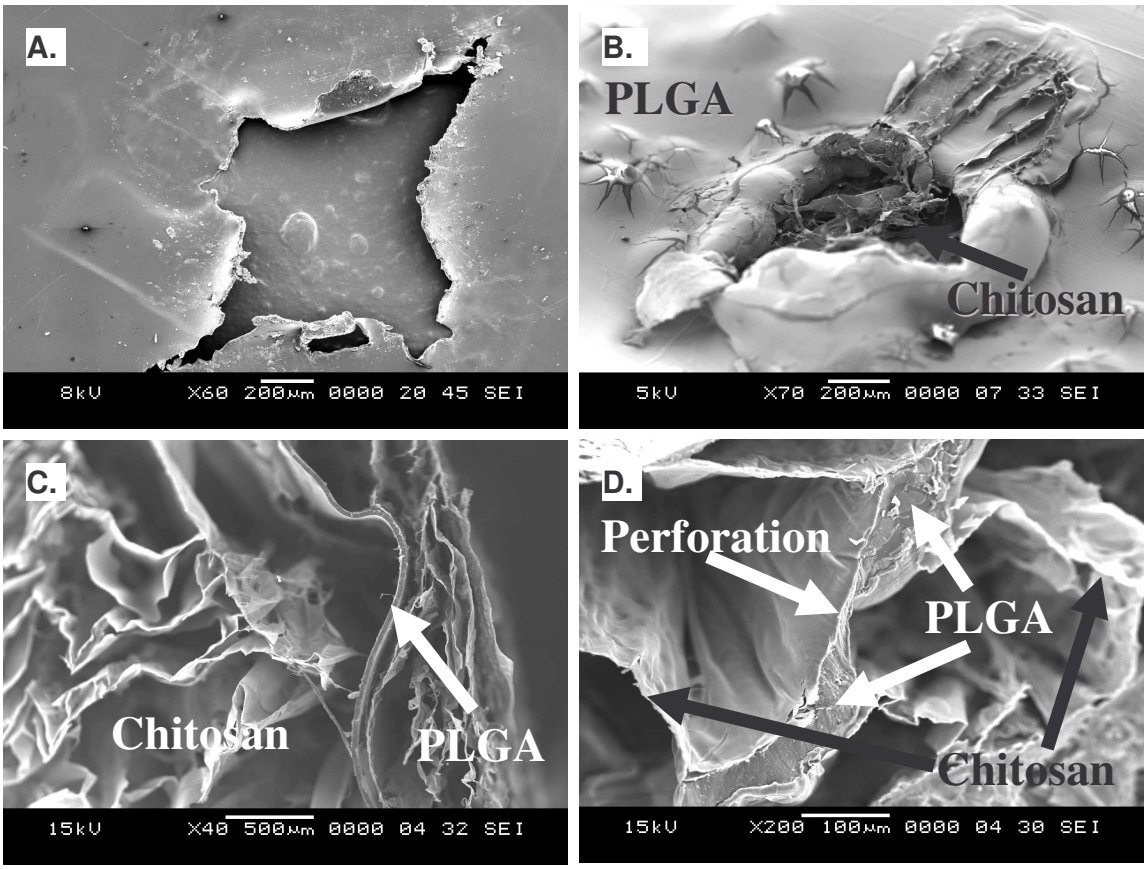

Figure 11. Composite Scaffold Structure during Fabrication

Panel A. SEM Micrograph of a perforation made in the PLGA film . Panel B. SEM Micrograph of a perforation in the 2 layer Chitosan-PLGA structure Panel C. SEM micrograph of the composite structure. Panel D. SEM micrograph showing that the porous chitosan layer is continuous through a perforation in the PLGA.

Tensile Properties

An average thickness of the dry PLGA films (50 μm) was used in the stress calculations of all materials PLGA films with and without perforations, and the composite. The 50 μm thickness was used in order to directly evaluate the effect of different processing steps on the tensile properties of PLGA. Further, there were issues in accurately measuring the thickness in the composite structures. At 4x magnification the entire scaffold is too large to visualize under the light microscope, the porous layer thickness varies when it is cut, and because the scaffold is soft it deforms when measured with a micrometer. The composite structure has a break stress between 3.5 and 5 MPa which is comparable to the tensile stress of distal SIS (3MPa) [36] (**Figure 12**). The stress strain curves are non-linear, and the composite structure stretches more than SIS before it breaks. The stress strain curve for the composite also shows the point where the chitosan layer fails. The small perturbations caused by the chitosan failure show that the majority of the composite scaffold's mechanical strength comes from the PLGA layer. The modulus of elasticity in the initial linear range (<80% strain) for the trilayer material is 28.7 ± 7.6 KPa, and the modulus of elasticity for PLGA films is 12.8 ± 3.7 KPa. The chitosan layers broke in a tiled pattern, and the chitosan tiles remained attached to the PLGA at the site of the perforations. This can be seen as breaks in the stress strain curve (**Figure 12**).

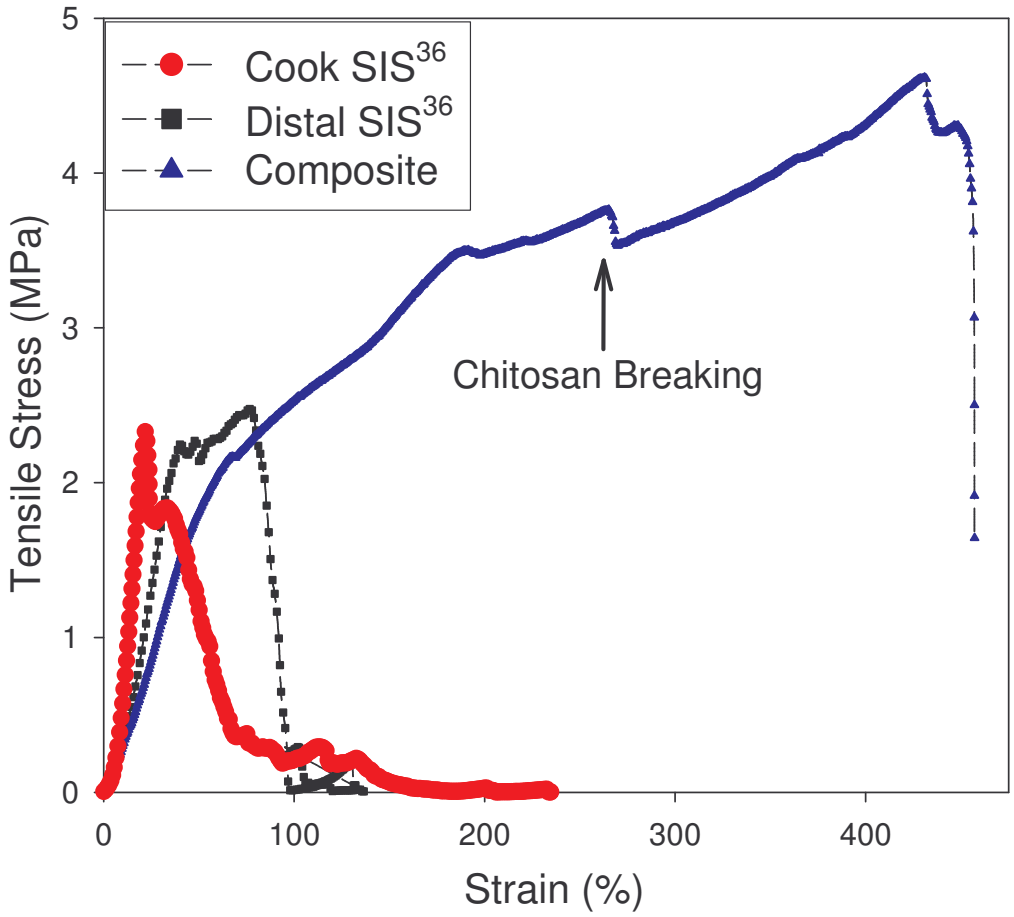

Figure 12. Stress Strain Behavior of SIS and Composite

Permeability to Urea

The composite scaffold is much less permeable to urea than SIS. After 8 hours, the final concentration of urea that had diffused through the composite is 80 mM while urea diffusing SIS reaches that concentration less than 30 minutes (**Figure 13**). Additionally, the 80 mM final concentration is only 30% of the expected equilibrium concentration of 275 mM, and after 8 hours the concentration of urea the initial side was approximately 300 mM. When the data was fitted with trend lines the SIS data showed exponential growth to a maximum while the composite structure trend was a quadratic polynomial.

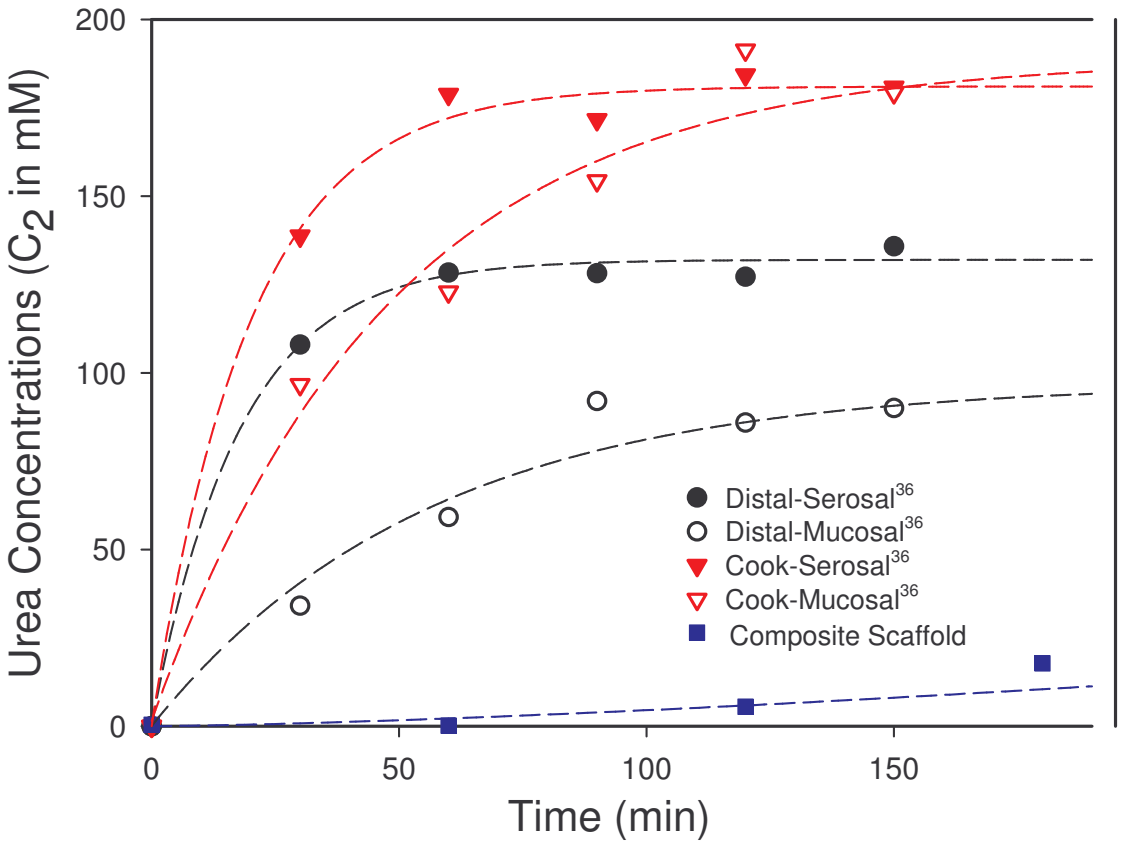

Figure 13. Diffusion of Urea Across Composite Membrane

Scaffold Degradation

To evaluate the degredation characteristics of the composite scaffolds, samples were incubated PBS containing in lysozyme, the enzyme that degrades chitosan. These results showed no significant change in dimension when analyzed by SEM at different time points. The composite scaffolds maintain both layered and porous structures during degradation (**Figure 14**). This retention of structure is important because the layered structure provides mechanical strength to the composite and the porous structure enhances cellular growth. The scaffolds showed minimal mass loss over 4 weeks (**Figure 15**). Some of the losses were caused by the samples sticking to the well plates. Several samples proved difficult to remove. The solution pH drops from 7.4 to 6.8 in one

day and remains steady at 6.8 for the next 7 days. This is caused by the PBS being incubated in a CO_2 environment, as shown by a PBS control in **Figure 16**.

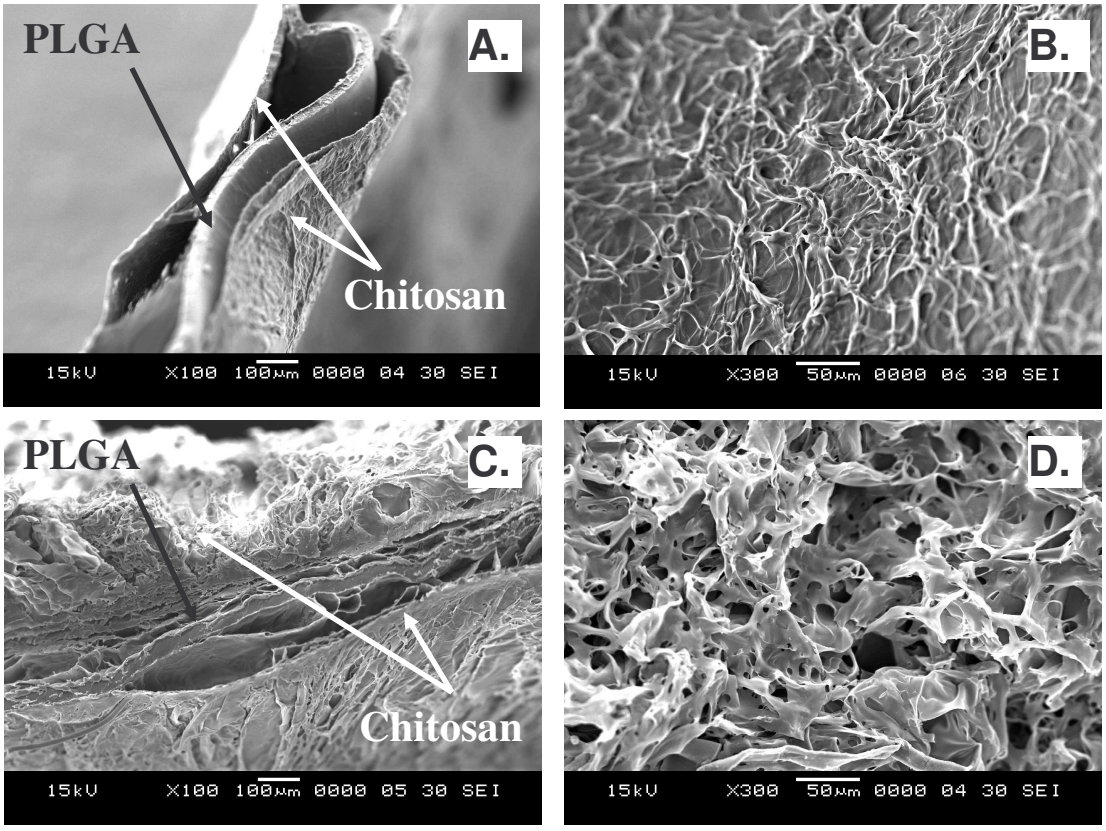

Figure 14. Composite Membranes Retain their 3D Structure during Degradation

Panel A. Cross Sectional View of the Composite Membrane after 3 days in PBS, Panel B. Top View of the Composite Membrane after 3 days in PBS, Panel C. Cross Sectional View of the Composite Membrane after 21 days in PBS, Panel D. Top View of the Composite Membrane after 21 days in PBS

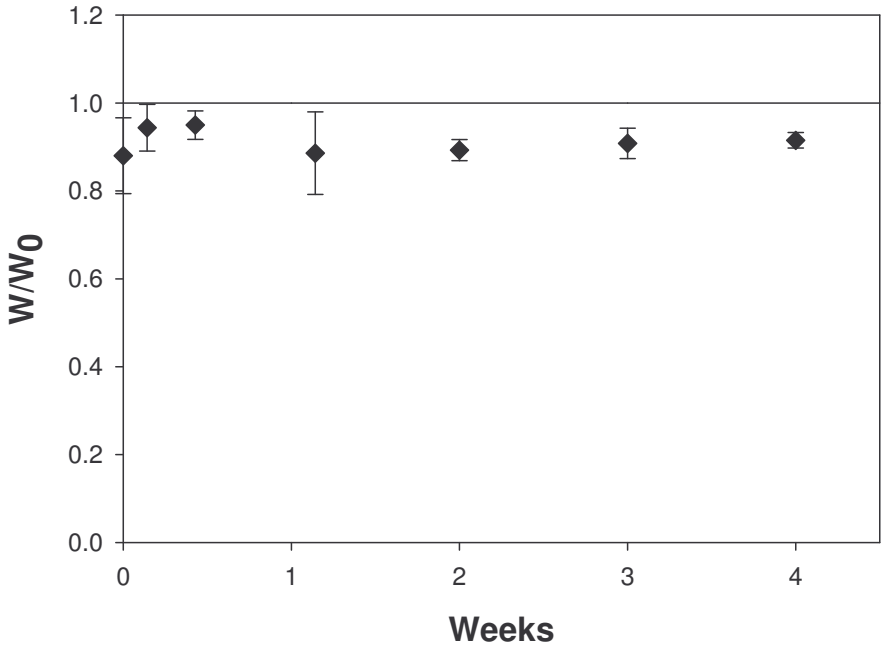

Figure 15. Mass Loss during the Degradation Experiment

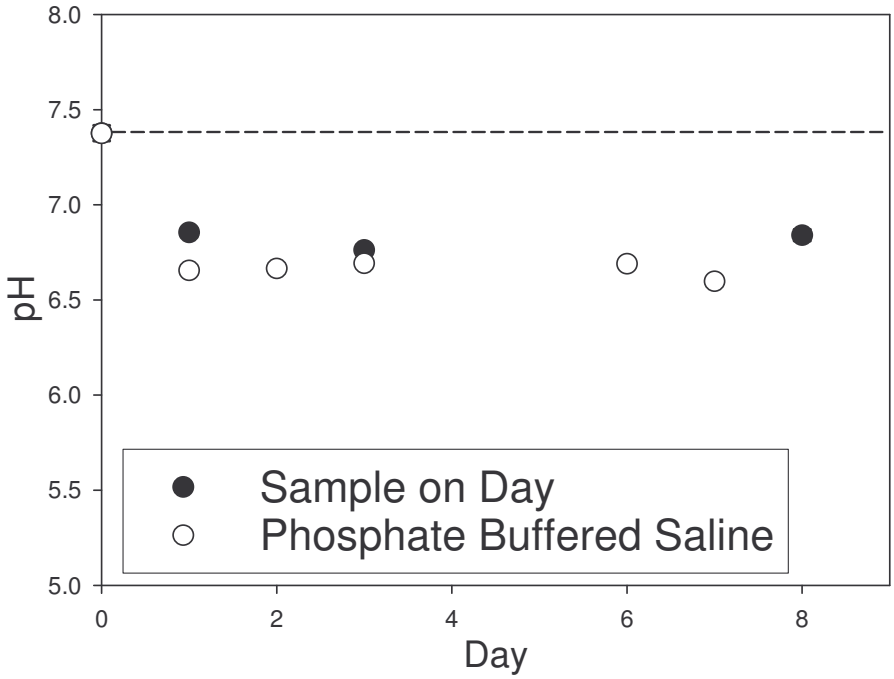

Figure 16. pH change during Degradation Experiment

Cell Culture

Data shows that cells will colonize the composite scaffold (**Figure 17**.) Two days after cell seeding, many cells had attached to the tissue culture plastic (TCP) surfaces in wells containing PLGA (with and without perforations). However, significantly fewer cells had attached to TCP surfaces in wells containing composite scaffolds. This indicates that the cells are attached to the composite membrane, but not to the PLGA film.

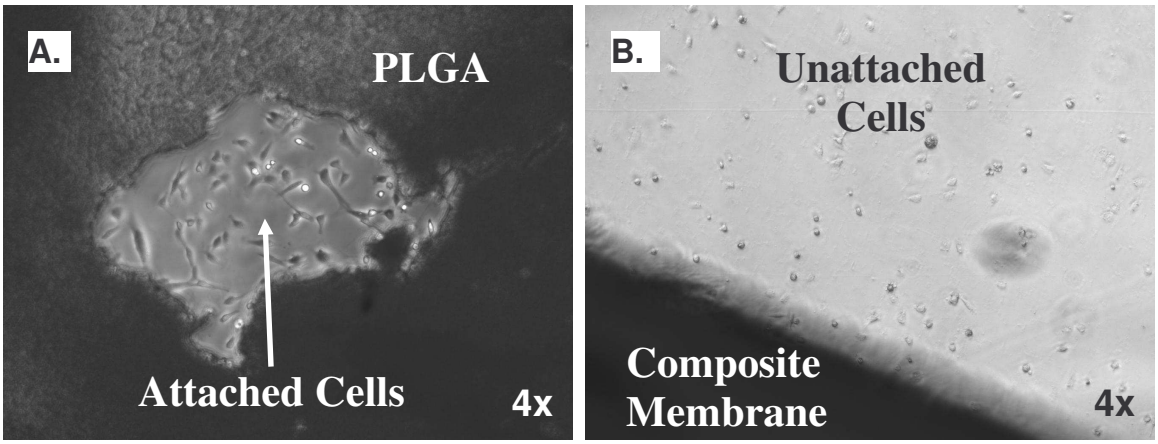

Figure 17. Cells Attach to the Composite Membrane but not to PLGA

Panel A. Cells adhere to the tissue culture plastic in well containing PLGA films with perforations. Panel B. Cells do not adhere to the tissue culture plastic in well containing the composite membranes.

V. Conclusions

This study explored the development of a novel process for generating composite scaffolds containing both natural and synthetic polymers. Further, properties of the scaffolds were evaluated and compared to naturally occurring SIS. The scaffolds were formed in a layered configuration consisting of a PLGA layer surrounded by two porous chitosan layers. The hydrophobic PLGA layer was perforated and the hydrophilic chitosan layer was continuous through the perforations, anchoring the three layers together. SEM micrographs show that the composite contains both the layered and porous structural elements. Composite scaffolds have thicknesses on the order of 2 mm, ten times the thickness of SIS. The increased thickness is due to the chitosan solution pooling on the hydrophobic PLGA.

The composite has mechanical properties similar to SIS [36]. It exhibits non-linear behavior and has a tensile stress greater than SIS. The PLGA layer retains its mechanical strength in a composite scaffold, and remains mechanically sound under tensile loading. The composite does not delaminate with the chitosan layers remaining firmly anchored at the perforations.

The composite also proved to be less permeable to urea than SIS [36]. Over 8 hour contact times the final concentration of urea that has diffusing through the composites is 80 mM while in SIS urea reaches similar concentrations in only 30 minutes. This is beneficial because a less permeable scaffold will leak less nitrogenous waste into surrounding tissues.

Over the course of 4 weeks, composite scaffold degradation was minimal. pH profiles during degradation experiments match profiles for the PBS control, demonstrating that the composite scaffold does not leach acidic byproducts. The composite scaffold retains both the layered and porous structural elements throughout the degradation run.

The composite scaffolds show good potential for cell colonization. Two days after cell seeding, many cells had attached to the tissue culture plastic (TCP) surfaces in wells containing PLGA (with and without perforations). However, significantly fewer cells had attached to TCP surfaces in wells containing composite scaffolds. This shows that cells attach to the composite structure more readily than to PLGA films.

The composite scaffold shows significant potential for use in tissue engineering applications. The composite contains both layered and porous structural features and provides suitable mechanical properties. The scaffold is relatively impermeable to urea. The composite demonstrates the capacity for cell colonization and the potential for cell growth.

VI. Recommendations and Future Directions

In light of current successes, the next phase of the project should focus on, modifying the process for use in other polymer systems, increasing the biological activity of the composite, modeling mass transfer through the scaffold, and utilizing the process as a platform technology to create custom multilayer scaffolds for a variety of tissue engineering applications. These studies continue the process toward the overall goal of generating a patentable material, approved by the FDA, for improved treatment of bladder defects and diseases.

The scaffold physical properties should be examined further. Since the majority of the biological loading is cyclical, cyclic tests should be performed to measure and model the viscoelastic properties of the composite. The effect of the perforations should also be investigated. The effect of both perforation size and spacing on the composite's physical properties should be investigated. Permeability studies should be conducted to determine if the permeability is primarily controlled by the number of perforations, the thickness and porosity of the chitosan layer, or both. Also, the degradation kinetics of the composite scaffold should be investigated further, including a long term degradation study and changes in scaffold dimensions during degradation. Further studies should be conducted to exploring methods to decrease the thickness of the composite. Reducing the hydrophobicity of the PLGA layer through nano-etching with a base[47] or decreasing the surface tension of the chitosan solution with detergents (SDS, Triton-X 100).

Additionally, the scaffold thickness could be made more uniform by adding a final pressing step to the process.

The method of composite scaffold construction is not limited solely to the PLGA and chitosan system. The central polymer film can be created by any desired method, and the outer layers can be added provided the solvent does not dissolve the central layer. Additional studies utilizing other polymers (PCL, PLA, PGA, gelatin, etc) should be performed to analyze the effectiveness of this method as a platform technology. For example, a scaffold containing low molecular weight PCL and gelatin would provide faster degradation. Scaffolds containing PCL and a blend of chitosan and gelatin could possibly improve bioactivity. It may also be possible to form a two layer asymmetric matrix using a PCL and chitosan. Additionally, PCL membranes can be constructed in non-planar geometries using techniques developed in our laboratory by others (data unpublished). Ideally, the system will be adapted to produce spherical scaffolds. Standard photolithographic methods could also be used to fabricate composite scaffolds. Photolithography will enable more precise control of the perforation pattern and scaffold micro-structure. Additionally, photolithographic techniques have already been developed for industrial scale processing. Biological activity could be enhanced by using either gelatin or blended chitosan/gelatin hydrogels instead of the 3D porous chitosan.

This study explored cellular adhesion and short term cell viability. The study needs to be expanded to include long term viability and quality of the remodeled tissue. Additionally, the composite should be optimized to increase its biological activity. The composite should be seeded with smooth muscle cells, and then analyzed for cellular growth, proliferation, and organization. The multilayer design also shows the potential to

grow multiple tissue layers simultaneously. Smooth muscle cells may be seeded onto one side of the composite while urothelial cells are seeded on the other. The central layer should provide a barrier between the two tissue compartments, preventing ingrowth of one cell type into the other until both regenerated tissues have time to organize themselves. Degradable nano-particles may be incorporated within the scaffold in order to release growth factors. These growth factors can also be incorporated into either a central PLGA layer or outer hydrogels layers and their release will be controlled by the degradation rate of the composite. The system may be applicable for the regeneration of other heterogeneous tissues.

The system should be modeled to determine the mass transfer coefficients for both Urea and oxygen. After optimizing scaffold construction scale up and mass production issues will have to be addressed. A bioreactor experiment should be performed to model the transport of both oxygen and urea across the scaffold. Then using the mass transfer coefficient the system can be simulated, including oxygen consumption, in order to evaluate and optimize a variety of spherical bioreactor designs.

This research shows great potential to expand the realm of tissue engineering. In time they may lower the demand for donor tissues and organs, and these studies should help improve the treatment of bladder defects and diseases.

References

1. Oberpenning F, Meng J, Yoo JJ, Atala A. De novo reconstitution of a functional mammalian urinary bladder by tissue engineering. Nat Biotechnol 1999;17(2):149-55.
2. Duel BP, Gonzalez R, Barthold JS. Alternative techniques for augmentation cystoplasty. J Urol 1998;159(3):998-1005.
3. Skinner DG, Boyd SD, Lieskovsky G. Clinical experience with the Kock continent ileal reservoir for urinary diversion. J Urol 1984;132(6):1101-7.
4. Khoury JM, Timmons SL, Corbel L, Webster GD. Complications of enterocystoplasty. Urology 1992;40(1):9-14.
5. Gleeson MJ, Griffith DP. The use of alloplastic biomaterials in bladder substitution. J Urol 1992;148(5):1377-82.
6. Langer R, Vacanti JP. Tissue engineering. Science 1993;260(5110):920-6.
7. Persidis A. Tissue engineering. Nat Biotechnol 1999;17:508-510.
8. Vyavahare N, Ogle M, Schoen FJ, Zand R, Gloeckner DC, Sacks M, Levy RJ. Mechanisms of bioprosthetic heart valve failure: fatigue causes collagen denaturation and glycosaminoglycan loss. J Biomed Mater Res 1999;46(1):44-50.
9. Chvapil M. Collagen sponge: theory and practice of medical applications. Journal of Biomedical Materials Research 1977;11(5):721-741.
10. Medalie DA, Eming SA, Tompkins RG, Yarmush ML, Krueger GG, Morgan JR. Evaluation of human skin reconstituted from composite grafts of cultured keratinocytes and human acellular dermis transplanted to athymic mice. J Invest Dermatol 1996;107(1):121-7.
11. Feng X, Tan J, Pan Y, Wu Q, Ruana S, Shena R, Chena X, Dua Y. Control of hypertrophic scar from inception by using xenogenic (porcine) acellular dermal matrix (ADM) to cover deep second degree burn. Burns 2006;32(3):293-298.
12. Kropp BP. Small-intestinal submucosa for bladder augmentation: a review of preclinical studies. World J Urol 1998;16(4):262-7.
13. Badylak SF, Record R, Lindberg K, Hodde J, Park K. Small intestinal submucosa: a substrate for in vitro cell growth. J Biomater Sci Polym Ed 1998;9(8):863-78.
14. Pariente JL, Kim BS, Atala A. In vitro biocompatibility evaluation of naturally derived and synthetic biomaterials using normal human bladder smooth muscle cells. J Urol 2002;167(4):1867-71.
15. Hiles MC, Badylak SF, Lantz GC, Kokini K, Geddes LA, Morff RJ. Mechanical properties of xenogeneic small-intestinal submucosa when used as an aortic graft in the dog. J Biomed Mater Res 1995;29(7):883-91.
16. Badylak SF, Kropp B, McPherson T, Liang H, Snyder PW. Small intestional submucosa: a rapidly resorbed bioscaffold for augmentation cystoplasty in a dog model. Tissue Eng 1998;4(4):379-87.

17. Allman AJ, McPherson TB, Badylak SF, Merrill LC, Kallakury B, Sheehan C, Raeder RH, Metzger DW. Xenogeneic extracellular matrix grafts elicit a TH2-restricted immune response. Transplantation 2001;71(11):1631-1640.
18. Badylak SF, Lantz GC, Coffey A, Geddes LA. Small intestinal submucosa as a large diameter vascular graft in the dog. The Journal Of Surgical Research 1989;47(1):74-80.
19. Pavcnik D, Uchida BT, Timmermans HA, Corless CL, O'Hara M, Toyota N, Moneta GL, Keller FS, Rosch J. Percutaneous bioprosthetic venous valve: a long-term study in sheep. J Vasc Surg 2002;35(3):598-602.
20. Brountzos E, Pavcnik D, Timmermans HA, Corless C, Uchida BT, Nihsen ES, Nakata M, Schoder M, Kaufman JA, Keller FS and others. Remodeling of suspended small intestinal submucosa venous valve: an experimental study in sheep to assess the host cells' origin. J Vasc Interv Radiol 2003;14(3):349-56.
21. Matheny RG, Hutchison ML, Dryden PE, Hiles MD, Shaar CJ. Porcine small intestine submucosa as a pulmonary valve leaflet substitute. J Heart Valve Dis 2000;9(6):769-74; discussion 774-5.
22. Bello YM, Falabella AF, Eaglstein WH. Tissue-engineered skin. Current status in wound healing. Am J Clin Dermatol 2001;2(5):305-13.
23. Badylak SF, Tullius R, Kokini K, Shelbourne KD, Klootwyk T, Voytik SL, Kraine MR, Simmons C. The use of xenogeneic small intestinal submucosa as a biomaterial for Achilles tendon repair in a dog model. Journal Of Biomedical Materials Research 1995;29(8):977-985.
24. Prevel CD, Eppley BL, Summerlin DJ, Sidner R, Jackson JR, McCarty M, Badylak SF. Small intestinal submucosa: utilization as a wound dressing in full-thickness rodent wounds. Ann Plast Surg 1995;35(4):381-8.
25. Nuininga JE, Moerkerk H, Hanssen A, Hulsbergen CA, Oosterwijk-Wakka J, Oosterwijk E, de Gier RP, Schalken JA, Kuppevelt TH, Feitz WF. A rabbit model to tissue engineer the bladder. Biomaterials 2004;25(9):1657-61.
26. Cheng EY, Kropp BP. Urologic tissue engineering with small-intestinal submucosa: potential clinical applications. World J Urol 2000;18(1):26-30.
27. Colvert JR, 3rd, Kropp BP, Cheng EY, Pope JCt, Brock JW, 3rd, Adams MC, Austin P, Furness PD, 3rd, Koyle MA. The use of small intestinal submucosa as an off-the-shelf urethral sling material for pediatric urinary incontinence. J Urol 2002;168(4 Pt 2):1872-5; discussion 1875-6.
28. Smith TG, 3rd, Gettman M, Lindberg G, Napper C, Pearle MS, Cadeddu JA. Ureteral replacement using porcine small intestine submucosa in a porcine model. Urology 2002;60(5):931-4.
29. El-Assmy A, El-Hamid MA, Hafez AT. Urethral replacement: a comparison between small intestinal submucosa grafts and spontaneous regeneration. BJU Int 2004;94(7):1132-5.
30. Kropp BP, Cheng EY. Bioengineering organs using small intestinal submucosa scaffolds: in vivo tissue-engineering technology. J Endourol 2000;14(1):59-62.
31. Kropp BP. Small-intestinal submucosa for bladder augmentation: a review of preclinical studies.262-7.
32. Kropp BP, Rippy MK, Badylak SF, Adams MC, Keating MA, Rink RC, Thor KB. Regenerative urinary bladder augmentation using small intestinal submucosa:

urodynamic and histopathologic assessment in long-term canine bladder augmentations. J Urol 1996;155(6):2098-104.
33. Pope JCt, Davis MM, Smith ER, Jr., Walsh MJ, Ellison PK, Rink RC, Kropp BP. The ontogeny of canine small intestinal submucosa regenerated bladder. J Urol 1997;158(3 Pt 2):1105-10.
34. COOK Biotechnology. Customer Support (800) 457-4448, Accessed July 10, 2006
35. Kropp BP, Cheng EY, Lin H-K, Zhang Y. Reliable and reproducible bladder regeneration using unseeded distal small intestinal submucosa. Journal of Urology 2004;172((4 Pt 2)):1710-3.
36. Raghavan D, Kropp BP, Lin HK, Zhang Y, Cowan R, Madihally SV. Physical characteristics of small intestinal submucosa scaffolds are location-dependent. J Biomed Mater Res A 2005;73A(1):90-6.
37. Kropp BP, Rippy MK, Badylak SF, Adams MC, Keating MA, Rink RC, Thor KB. Regenerative urinary bladder augmentation using small intestinal submucosa: urodynamic and histopathologic assessment in long-term canine bladder augmentations. J Urol 1996;155(6):2098-104.
38. Huang Y, Siewe M, Madihally SV. Effect of spatial architecture on cellular colonization. Biotechnol Bioeng 2006;93(1):64-75.
39. Lee SH, Kim BS, Kim SH, Kang SW, Kim YH. Thermally produced biodegradable scaffolds for cartilage tissue engineering. Macromol Biosci 2004;4(8):802-10.
40. Mooney DJ, Baldwin DF, Suh NP, Vacanti JP, Langer R. Novel approach to fabricate porous sponges of poly(D,L-lactic-co-glycolic acid) without the use of organic solvents. Biomaterials 1996;17(14):1417-22.
41. Riddle KW, Mooney DJ. Role of poly(lactide-co-glycolide) particle size on gas-foamed scaffolds. J Biomater Sci Polym Ed 2004;15(12):1561-70.
42. Chun KW, Cho KC, Kim SH, Jeong JH, Park TG. Controlled release of plasmid DNA from biodegradable scaffolds fabricated using a thermally-induced phase-separation method. J Biomater Sci Polym Ed 2004;15(11):1341-53.
43. Mikos AG, Thorsen AJ, Czerwonka LA, Bao Y, Langer R, Winslow DN, Vacanti JP. Preparation and characterization of poly(L-lactic acid) foams. Polymer 1994;35(5):1068-1077.
44. Smay JE, Nadkarni SS, Xu J, Wiist D, Madihally SV. Direct Writing of Multi-Material Structures using Colloidal Inks. Proceedings of 2006 NSF Design, Service, and Manufacturing Grantees and Research Conference, St. Louis, Missouri 2006.
45. Yang YB, S.; Tomasko, D. L.; Lee, L. J.; Yang, S. Fabrication of well-defined PLGA scaffolds using novel microembossing and carbon dioxide bonding. Biomaterials 2005;26(15):2585–2594.
46. Yang RC, T.; Chen, H.; Wang, W. Microfabrication of biodegradable (PLGA) honeycomb-structures and potential applications in implantable drug delivery. Sensors and Actuators B: Chemical 2005;106(2):506-511.
47. Thapa AM, D. C.; Webster,T. J.; Haberstroh, K. M. Nano-structured polymers enhance bladder smooth muscle cell function. Biomaterials 2003;24(17):2915-2926.

48. Pham QP, Sharma U, Mikos AG. Electrospinning of polymeric nanofibers for tissue engineering applications: a review. Tissue Engineering 2006;12(5):1197-1211.
49. Li WJ, Laurencin CT, Caterson EJ, Tuan RS, Ko FK. Electrospun nanofibrous structure: a novel scaffold for tissue engineering. J Biomed Mater Res 2002;60(4):613-21.
50. Lee CH, Shin HJ, Cho IH, Kang YM, Kim IA, Park KD, Shin JW. Nanofiber alignment and direction of mechanical strain affect the ECM production of human ACL fibroblast. Biomaterials 2005;26(11):1261-70.
51. Bryant SJ, Chowdhury TT, Lee DA, Bader DL, Anseth KS. Crosslinking density influences chondrocyte metabolism in dynamically loaded photocrosslinked poly(ethylene glycol) hydrogels. Annals of Biomedical Engineering 2004;32(3):407 - 417.
52. Chenite A, Chaput C, Wang D, Combes C, Buschmann MD, Hoeman CD, Leroux JC, Atkinson BL, Binette F, Selmani A. Novel injectable neutral solutions of chitosan form biodegradable gels in situ. Biomaterials 2000;21(21):2155-2161.
53. Nuttelman CR, Tripodi MC, Anseth KS. In vitro osteogenic differentiation of human mesenchymal stem cells photoencapsulated in PEG hydrogels. Journal of Biomedical Materials Research Part A 2004;68A(4):773 - 782.
54. Bryant SJ, Bender RJ, Durand KL, Anseth KS. Encapsulating chondrocytes in degrading PEG hydrogels with high modulus: Engineering gel structural changes to facilitate cartilaginous tissue production. Biotechnology and Bioengineering 2004;86(7):747 - 755.
55. Weber LM, He J, Bradley B, Haskins K, Anseth KS. PEG-based hydrogels as an in vitro encapsulation platform for testing controlled β-cell microenvironments. Acta Biomaterialia 2006;2(1):1-8.
56. Madihally SV, Matthew HW. Porous chitosan scaffolds for tissue engineering. Biomaterials 1999;20(12):1133-42.
57. Yamada KM, Pankov R, Cukierman E. Dimensions and dynamics in integrin function. Braz J Med Biol Res 2003;36(8):959-66. Epub 2003 Jul 23.
58. Wozniak MA, Modzelewska K, Kwong L, Keely PJ. Focal adhesion regulation of cell behavior. Biochim Biophys Acta 2004;1692(2-3):103-19.
59. Friedl P. Dynamic imaging of cellular interactions with extracellular matrix. Histochem Cell Biol 2004;122(3):183-90. Epub 2004 Jul 16.
60. Cukierman E, Pankov R, Stevens DR, Yamada KM. Taking cell-matrix adhesions to the third dimension. Science 2001;294(5547):1708-12.
61. Yannas IV, Lee E, Orgill DP, Skrabut EM, Murphy GF. Synthesis and characterization of a model extracellular matrix that induces partial regeneration of adult mammalian skin. Proc Natl Acad Sci U S A 1989;86(3):933-7.
62. Zeltinger J, Sherwood JK, Graham DA, Mueller R, Griffith LG. Effect of pore size and void fraction on cellular adhesion, proliferation, and matrix deposition. Tissue Engineering 2001;7(5):557-572.
63. Salem AK, Stevens R, Pearson RG, Davies MC, Tendler SJ, Roberts CJ, Williams PM, Shakesheff KM. Interactions of 3T3 fibroblasts and endothelial cells with defined pore features. J Biomed Mater Res 2002;61(2):212-7.

64. Ng KW, Khor HL, Hutmacher DW. In vitro characterization of natural and synthetic dermal matrices cultured with human dermal fibroblasts. Biomaterials 2004;25(14):2807-18.
65. Wang YC, Ho CC. Micropatterning of proteins and mammalian cells on biomaterials. Faseb J 2004;18(3):525-7. Epub 2004 Jan 8.
66. Ranucci CS, Kumar A, Batra SP, Moghe PV. Control of hepatocyte function on collagen foams: sizing matrix pores toward selective induction of 2-D and 3-D cellular morphogenesis. Biomaterials 2000;21(8):783-93.
67. Lavik E, Teng YD, Snyder E, Langer R. Seeding neural stem cells on scaffolds of PGA, PLA, and their copolymers. Methods Mol Biol 2002;198:89-97.
68. Nakamura T, Hitomi S, Watanabe S, Shimizu Y, Jamshidi K, Hyon SH, Ikada Y. Bioabsorption of polylactides with different molecular properties. J Biomed Mater Res 1989;23(10):1115-30.
69. Mooney DJ, Mazzoni CL, Breuer C, McNamara K, Hern D, Vacanti JP, Langer R. Stabilized polyglycolic acid fibre-based tubes for tissue engineering. Biomaterials 1996;17(2):115-24.
70. Gao J, Niklason L, Langer R. Surface hydrolysis of poly(glycolic acid) meshes increases the seeding density of vascular smooth muscle cells. J Biomed Mater Res 1998;42(3):417-24.
71. Marra KG, Szem JW, Kumta PN, DiMilla PA, Weiss LE. In vitro analysis of biodegradable polymer blend/hydroxyapatite composites for bone tissue engineering. J Biomed Mater Res 1999;47(3):324-35.
72. Engelberg I, Kohn J. Physico-mechanical properties of degradable polymers used in medical applications: a comparative study. Biomaterials 1991;12(3):292-304.
73. Ozawa T, Mickle DA, Weisel RD, Koyama N, Wong H, Ozawa S, Li RK. Histologic changes of nonbiodegradable and biodegradable biomaterials used to repair right ventricular heart defects in rats. J Thorac Cardiovasc Surg 2002;124(6):1157-64.
74. Hutmacher DW, Schantz T, Zein I, Ng KW, Teoh SH, Tan KC. Mechanical properties and cell cultural response of polycaprolactone scaffolds designed and fabricated via fused deposition modeling. J Biomed Mater Res 2001;55(2):203-16.
75. Lowry KJ, Hamson KR, Bear L, Peng YB, Calaluce R, Evans ML, Anglen JO, Allen WC. Polycaprolactone/glass bioabsorbable implant in a rabbit humerus fracture model. J Biomed Mater Res 1997;36(4):536-41.
76. Kulkarni RK, Moore EG, Hegyeli AF, Leonard F. Biodegradable poly(lactic acid) polymers. J Biomed Mater Res 1971;5(3):169-81.
77. Saito N, Okada T, Toba S, Miyamoto S, Takaoka K. New synthetic absorbable polymers as BMP carriers: plastic properties of poly-D,L-lactic acid-polyethylene glycol block copolymers. J Biomed Mater Res 1999;47(1):104-10.
78. Park IK, Yang J, Jeong HJ, Bom HS, Harada I, Akaike T, Kim SI, Cho CS. Galactosylated chitosan as a synthetic extracellular matrix for hepatocytes attachment. Biomaterials 2003;24(13):2331-7.
79. Ho KL, Witte MN, Bird ET. 8-ply small intestinal submucosa tension-free sling: spectrum of postoperative inflammation. J Urol 2004;171(1):268-71.

80. Pistner H, Bendix DR, Muhling J, Reuther JF. Poly(L-lactide): a long-term degradation study in vivo. Part III. Analytical characterization. Biomaterials 1993;14(4):291-8.
81. Kranz H, Ubrich N, Maincent P, Bodmeier R. Physicomechanical properties of biodegradable poly(D,L-lactide) and poly(D,L-lactide-co-glycolide) films in the dry and wet states. J Pharm Sci 2000;89(12):1558-66.
82. Yoon JJ, Park TG. Degradation behaviors of biodegradable macroporous scaffolds prepared by gas foaming of effervescent salts. J Biomed Mater Res 2001;55(3):401-8.
83. Lu L, Peter SJ, Lyman MD, Lai HL, Leite SM, Tamada JA, Uyama S, Vacanti JP, Langer R, Mikos AG. In vitro and in vivo degradation of porous poly(DL-lactic-co-glycolic acid) foams. Biomaterials 2000;21(18):1837-45.
84. Seal BL, Otero TC, Panitch A. Polymeric biomaterials for tissue and organ regeration. Materials Science and Engineering 2001;34:147-230.
85. Xue L, Greisler HP. Biomaterials in the development and future of vascular grafts. J Vasc Surg 2003;37(2):472-80.
86. Gunatillake PA, Adhikari R. Biodegradable synthetic polymers for tissue engineering. Eur Cell Mater 2003;5:1-16; discussion 16.
87. Middleton JC, Tipton AJ. Synthetic biodegradable polymers as orthopedic devices. Biomaterials 2000;21(23):2335-46.
88. Korossis SA, Booth C, Wilcox HE, Watterson KG, Kearney JN, Fisher J, Ingham E. Tissue engineering of cardiac valve prostheses II: biomechanical characterization of decellularized porcine aortic heart valves. J Heart Valve Dis 2002;11(4):463-71.
89. Massia SP, Hubbell JA. Covalently attached GRGD on polymer surfaces promotes biospecific adhesion of mammalian cells. Ann N Y Acad Sci 1990;589:261-70.
90. Agrawal CM, Athanasiou KA. Technique to control pH in vicinity of biodegrading PLA-PGA implants. J Biomed Mater Res 1997;38(2):105-14.
91. Park A, Wu B, Griffith LG. Integration of surface modification and 3D fabrication techniques to prepare patterned poly(L-lactide) substrates allowing regionally selective cell adhesion. J Biomater Sci Polym Ed 1998;9(2):89-110.
92. Eid K, Chen E, Griffith L, Glowacki J. Effect of RGD coating on osteocompatibility of PLGA-polymer disks in a rat tibial wound. J Biomed Mater Res 2001;57(2):224-31.
93. Risbud MV, Hardikar AA, Bhat SV, Bhonde RR. pH-sensitive freeze-dried chitosan-polyvinyl pyrrolidone hydrogels as controlled release system for antibiotic delivery. J Control Release 2000;68(1):23-30.
94. Suh JK, Matthew HW. Application of chitosan-based polysaccharide biomaterials in cartilage tissue engineering: a review. Biomaterials 2000;21(24):2589-98.
95. Huang Y, Onyeri S, Siewe M, Moshfeghian A, Madihally SV. In vitro characterization of chitosan-gelatin scaffolds for tissue engineering. Biomaterials 2005;26(36):7616-27.
96. Malafaya PB, Pedro AJ, Peterbauer A, Gabriel C, Redl H, Reis RL. Chitosan particles agglomerated scaffolds for cartilage and osteochondral tissue

engineering approaches with adipose tissue derived stem cells. Journal of Materials Science: Materials in Medicine 2005;16(12):1077 - 1085.
97. Lahiji A, Sohrabi A, Hungerford DS, Frondoza CG. Chitosan supports the expression of extracellular matrix proteins in human osteoblasts and chondrocytes. J Biomed Mater Res 2000;51(4):586-95.
98. Wang XH, Li DP, Wang WJ, Feng QL, Cui FZ, Xu YX, Song XH, van der Werf M. Crosslinked collagen/chitosan matrix for artificial livers. Biomaterials 2003;24(19):3213-20.
99. Yuan Y, Zhang P, Yang Y, Wang X, Gu X. The interaction of Schwann cells with chitosan membranes and fibers in vitro. Biomaterials 2004;25(18):4273-4278.
100. Wenling C, Duohui J, Jiamou L, Yandao G, Nanming Z, Xiufang Z. Effects of the degree of deacetylation on the physicochemical properties and Schwann cell affinity of chitosan films. Journal of biomaterials applications 2005;20(2):157-77.
101. Ehrenfreund-Kleinman T, A.J. D, Golenser J. Polysaccharide Scaffolds Prepared by Crosslinking of Polysaccharides with Chitosan or Proteins for Cell Growth. J Bioact Compat Polym 2003;18(5):323-338.
102. Mei N, Chen G, Zhou P, Chen X, Shao ZZ, Pan LF, Wu CG. Biocompatibility of Poly(epsilon-caprolactone) scaffold modified by chitosan--the fibroblasts proliferation in vitro. J Biomater Appl 2005;19(4):323-39.
103. Lee JY, Spicer AP. Hyaluronan: a multifunctional, megaDalton, stealth molecule. Curr Opin Cell Biol 2000;12(5):581-6.
104. Tadmor R, Chen N, Israelachvili JN. Thin film rheology and lubricity of hyaluronic acid solutions at a normal physiological concentration. J Biomed Mater Res 2002;61(4):514-23.
105. Tam EM, Wu YI, Butler GS, Stack MS, Overall CM. Collagen binding properties of the membrane type-1 matrix metalloproteinase (MT1-MMP) hemopexin C domain. The ectodomain of the 44-kDa autocatalytic product of MT1-MMP inhibits cell invasion by disrupting native type I collagen cleavage. J Biol Chem 2002;277(41):39005-14. Epub 2002 Jul 26.
106. Mao J, Zhao L, De Yao K, Shang Q, Yang G, Cao Y. Study of novel chitosan-gelatin artificial skin in vitro. J Biomed Mater Res 2003;64A(2):301-8.
107. Xiao Y, Qian H, Young WG, Bartold PM. Tissue engineering for bone regeneration using differentiated alveolar bone cells in collagen scaffolds. Tissue Eng 2003;9(6):1167-77.
108. Westreich R, Kaufman M, Gannon P, Lawson W. Validating the subcutaneous model of injectable autologous cartilage using a fibrin glue scaffold. Laryngoscope 2004;114(12):2154-60.
109. Ting V, Sims CD, Brecht LE, McCarthy JG, Kasabian AK, Connelly PR, Elisseeff J, Gittes GK, Longaker MT. In vitro prefabrication of human cartilage shapes using fibrin glue and human chondrocytes. Ann Plast Surg 1998;40(4):413-20; discussion 420-1.
110. Griffith LG. Emerging design principles in biomaterials and scaffolds for tissue engineering. Ann N Y Acad Sci 2002;961:83-95.
111. Moshfegian A, Tillman J, Madihally S. Characterization of Emulsified Chitosan-PLGA Matrices Formed Using Controlled Rate Freezing and Lyophilization Technique. J. Biomedical Materials Research-Part A 2006(in press).

Table of Appendices

Appendix 1: Measuring PLGA Layer Thickness

The thickness of the PLGA layer was measured by first cutting the samples into 2 mm x 10 mm pieces. The pieces were placed on a glass microscope slide so the cross section was visible under an inverted microscope. A .jpg image was captured and imported into Sigma Scan Pro software. The length scale is set using a two point calibration on a hemocytometer (See **Figure 18**, the small squares have 250μm sides). Then the flim thickness can be measured as shown in **Figure 19**. Sample data for thickness measurements for membranes formed in Petri dishes and custom made square wells are shown in **Table 1** and **Table 2**.

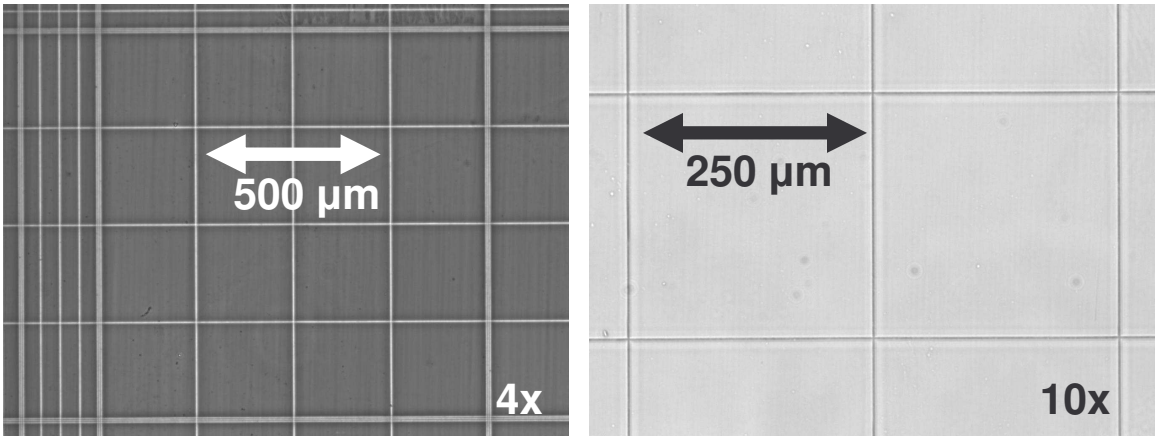

Figure 18. Images of the Hemocytometer used to Calibrate Sigma Scan Pro Software

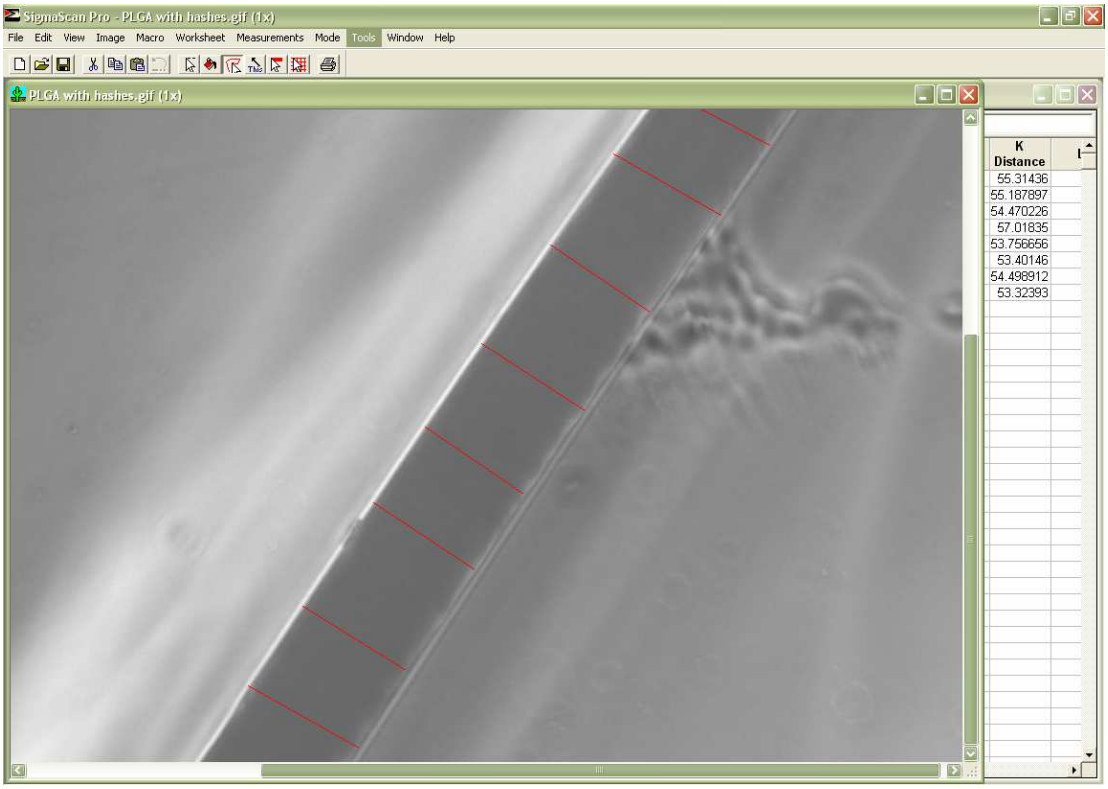

Figure 19. Measuring Sample Thickness Using Sigma Scan Pro

Point	Thickness (um)
1	70.6
2	71.57
3	68.71
4	67.81
5	68.31
6	69.17
7	61.1
8	61.66
9	66.68
10	65.91
11	56.49
12	63.73
13	61.55
14	68.89
15	72.5

Point	Thickness (um)
16	65.27
17	67.09
18	62.5
19	62.98
20	67.62
21	67.17
22	81.31
23	67.17
24	68.8
25	68.38
26	69.4
27	62.32
28	69.73
29	57.83
30	55.98
31	59.69

Point	Thickness (um)
32	61.55
33	55.99
34	56.39
35	66.07
36	58.67
37	61.72
38	60.19
39	58.21
40	60.56
41	59.77
42	60.56
43	58.2
44	57.96
45	58.99
46	56.93

Average	66.8
Standard Deviation	4.9

Table 1. Sample Thickness Data for Teflon Petri Dishes

Sample	Measurement	Thickness (um)	Sample	Measurement	Thickness (um)
1	1	51	10	1	40.4
1	2	49	10	2	35.3
1	3	50.8	10	3	34.5
1	4	52.2	10	4	30
1	5	49.9	10	5	35.9
2	1	54	11	1	38.8
2	2	53.9	11	2	47
2	3	52.4	11	3	41.8
2	4	49	11	4	45.4
2	5	49.1	11	5	41.8
3	1	41.2	12	1	39.3
3	2	40.2	12	2	39.3
3	3	36.5	12	3	46
3	4	44.6	12	4	51.9
3	5	41.7	12	5	43.1
4	1	43.5	13	1	33.1
4	2	39.9	13	2	34.6
4	3	37.6	13	3	33.1
4	4	40.4	13	4	34.1
4	5	34.5	13	5	36.2
5	1	51.1	14	1	52.3
5	2	47.5	14	2	58.9
5	3	50.8	14	3	70.5
5	4	47.4	14	4	81.7
5	5	47.6	14	5	88.3
6	1	40.9	15	1	50.5
6	2	46.2	15	2	54.1
6	3	43.5	15	3	52.1
6	4	40.8	15	4	53.5
6	5	39.5	15	5	51.1
7	1	49	16	1	96.7
7	2	51.7	16	2	97.1
7	3	54.6	16	3	91.3
7	4	54.7	16	4	84.1
7	5	54.6	16	5	94.3
8	1	40.4	17	1	93.1
8	2	38.2	17	2	78.4
8	3	39.5	17	3	67
8	4	34.3	17	4	47.4
8	5	39	17	5	39.2
9	1	29.2	18	1	45.1
9	2	27.7	18	2	39.3
9	3	30	18	3	33.5
9	4	30.7	18	4	37
9	5	30.1	18	5	32.3

Table 2. Sample Thickness Data using Custom Teflon-Silicon Wells

Sample	Measurement	Thickness (um)
19	1	34.7
19	2	38.1
19	3	34.7
19	4	39.3
19	5	39.3

Average	42.9
Standard Deviation	7.8

Table 3. Sample Thickness Data using Custom Teflon-Silicon Wells

Appendix 2: Stress-Strain Calculations and Data

Stress-strain measurements were taken in a hydrated condition using a custom designed chamber filled with PBS (**Figure 20**). Hydrated samples were cut into 1 cm x 6 cm sections, centered in the hydraulic grips (**Figure 21**), and pulled at a constant crosshead speed of 10mm/min. In order to directly compare the material the average PLGA film thickness (50μm) was used for all stress calculations. Sample data for PLGA films, perforated PLGA films, and the composite scaffold is shown in **Table 4**, **Table 5**, and **Table 6.**

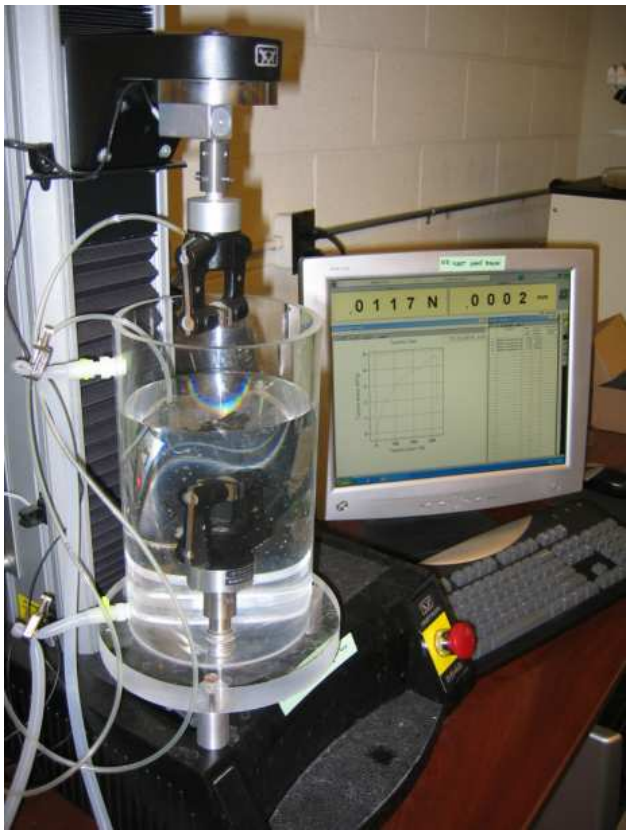

Figure 20. Custom Liquid Chamber used to Perform Mechanical Tests

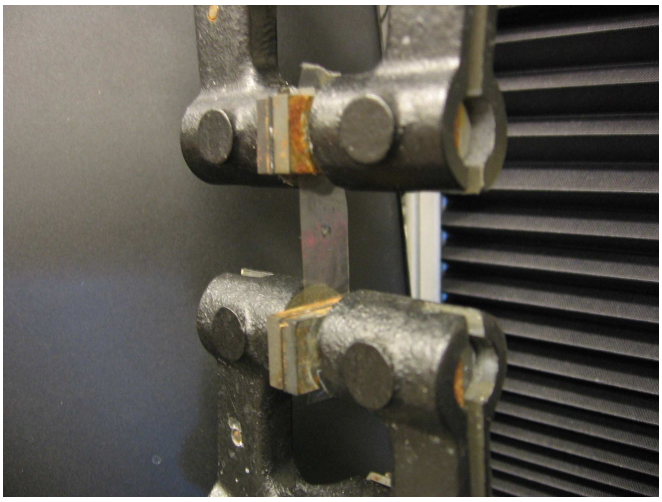

Figure 21. PLGA Film Inserted in the Mechanical Testing Device

Cook Strain %	Cook Stress MPa
Every Data Point Shown	
0.8	0.02
1.6	0.05
2.4	0.08
3.2	0.12
4.0	0.18
4.8	0.24
5.6	0.31
6.4	0.39
7.1	0.49
7.9	0.60
8.7	0.72
9.5	0.86
10.3	1.01
11.1	1.17
11.9	1.34
12.7	1.52
13.5	1.72
14.3	1.92
15.1	2.13
15.9	2.33
16.7	2.54
17.5	2.74
18.3	2.95

Cook Strain %	Cook Stress MPa
Every Data Point Shown	
19.1	3.14
19.8	3.33
20.6	3.50
21.4	3.64
22.2	3.73
23.0	3.77
23.8	3.73
24.6	3.64
25.4	3.60
26.2	3.58
27.0	3.58
27.8	3.60
28.6	3.57
29.4	3.57
30.2	3.49
31.0	3.35
31.7	3.12
32.5	2.97
33.2	2.69
33.8	2.41
34.2	2.13
34.4	1.84
34.7	1.56

Cook Strain %	Cook Stress MPa
Every Data Point Shown	
34.8	1.28
35.0	0.99
35.2	0.71
35.3	0.43
36.1	0.19
36.9	0.18
37.7	0.17
38.5	0.18
39.3	0.18
40.1	0.17
40.9	0.18
41.7	0.18
42.5	0.18
43.3	0.18
44.1	0.18
44.9	0.18
45.7	0.19
46.4	0.19
47.2	0.19
48.0	0.19
48.8	0.19
49.6	0.16
50.4	0.14

Table 4. Sample Stress-Strain Data for COOK SIS [36]

Distal Strain %	Distal Stress Mpa
Every 5th Data Point Shown	
4.2	0.02
8.1	0.07
12.1	0.19
16.1	0.42
20.0	0.77
20.8	0.85
24.8	1.33
28.8	1.91
32.7	2.58
36.7	3.27
37.5	3.41
41.5	4.07
45.4	4.62
49.4	4.91

Distal Strain %	Distal Stress Mpa
Every 5th Data Point Shown	
53.4	4.99
54.2	5.04
58.1	5.06
62.0	4.43
65.3	3.82
69.3	3.27
69.8	3.09
71.3	2.19
74.2	1.29
77.2	0.58
81.2	0.38
82.0	0.39
86.0	0.35

Distal Strain %	Distal Stress Mpa
Every 5th Data Point Shown	
89.9	0.25
93.9	0.22
97.9	0.26
98.7	0.26
102.6	0.29
106.6	0.06
110.6	0.05
114.5	0.06
115.3	0.07
119.3	0.09
123.3	0.12
127.2	0.17
131.2	0.04
132.0	0.04

Table 5. Sample Stress-Strain Data for Distal SIS [36]

Composite Strain %	Composite Stress Mpa
Every 10th Data Point Shown	
0	0.01
5	0.14
10	0.30
13	0.39
18	0.56
23	0.76
25	0.86
30	1.10
35	1.31
38	1.42
43	1.60
48	1.76
51	1.82
56	1.95
61	2.07
63	2.11
68	2.16
73	2.21
76	2.25
81	2.31
86	2.38
88	2.40
93	2.46
98	2.51
101	2.54
106	2.59
111	2.63
114	2.66
119	2.70
124	2.74
126	2.77
131	2.81
136	2.86
139	2.89
144	2.94
149	3.02
152	3.06

Composite Strain %	Composite Stress Mpa
Every 10th Data Point Shown	
157	3.13
162	3.20
164	3.23
169	3.30
174	3.36
177	3.39
182	3.45
187	3.48
189	3.50
194	3.48
199	3.48
202	3.49
207	3.51
212	3.52
215	3.54
220	3.56
225	3.55
227	3.57
232	3.59
237	3.61
240	3.63
245	3.65
250	3.68
253	3.69
258	3.73
263	3.76
265	3.76
270	3.53
275	3.56
278	3.58
283	3.61
288	3.63
290	3.64
295	3.66
301	3.68
303	3.70
308	3.72
313	3.75

Table 6. Sample Stress-Strain Data for the Composite Scaffold

Appendix 3: Scanning Electron Microscope

Sputter Coat the Sample with Gold

1. Apply a small coating of colloidal graphite to a clean stub
2. Place sample on carbon coating and let dry
3. Open the sputter coater chamber, insert stubs, and close chamber
4. Turn on the argon gas cylinder (counter-clockwise)
5. Turn on sputter coater and force down the lid to ensure a good seal
6. Push the “Manual” button
7. Wait for vacuum pressure to reach 0.02 mbar (takes 5 - 10 min)
8. Activate “Flush” for five seconds
9. Activate “Leak” for five seconds
10. Wait for pressure to reach 0.05 mbar
11. Press “Start” and allow coating for 30 - 60 seconds (To set time hold down pause/test button and use arrow keys)
12. Turn power off and close argon gas cylinder
13. Open the nitrogen gas cylinder to remove vacuum
14. Close nitrogen cylinder and remove stub

Operating the Scanning Electron Microscope

1. Open cooling water valve
2. Turn on computer and open SEM main menu
3. Go to the “Sample” menu and click “Vent”
4. When the vent light stops flashing, open the SEM chamber and insert the sample
5. Close chamber and press “Evac”

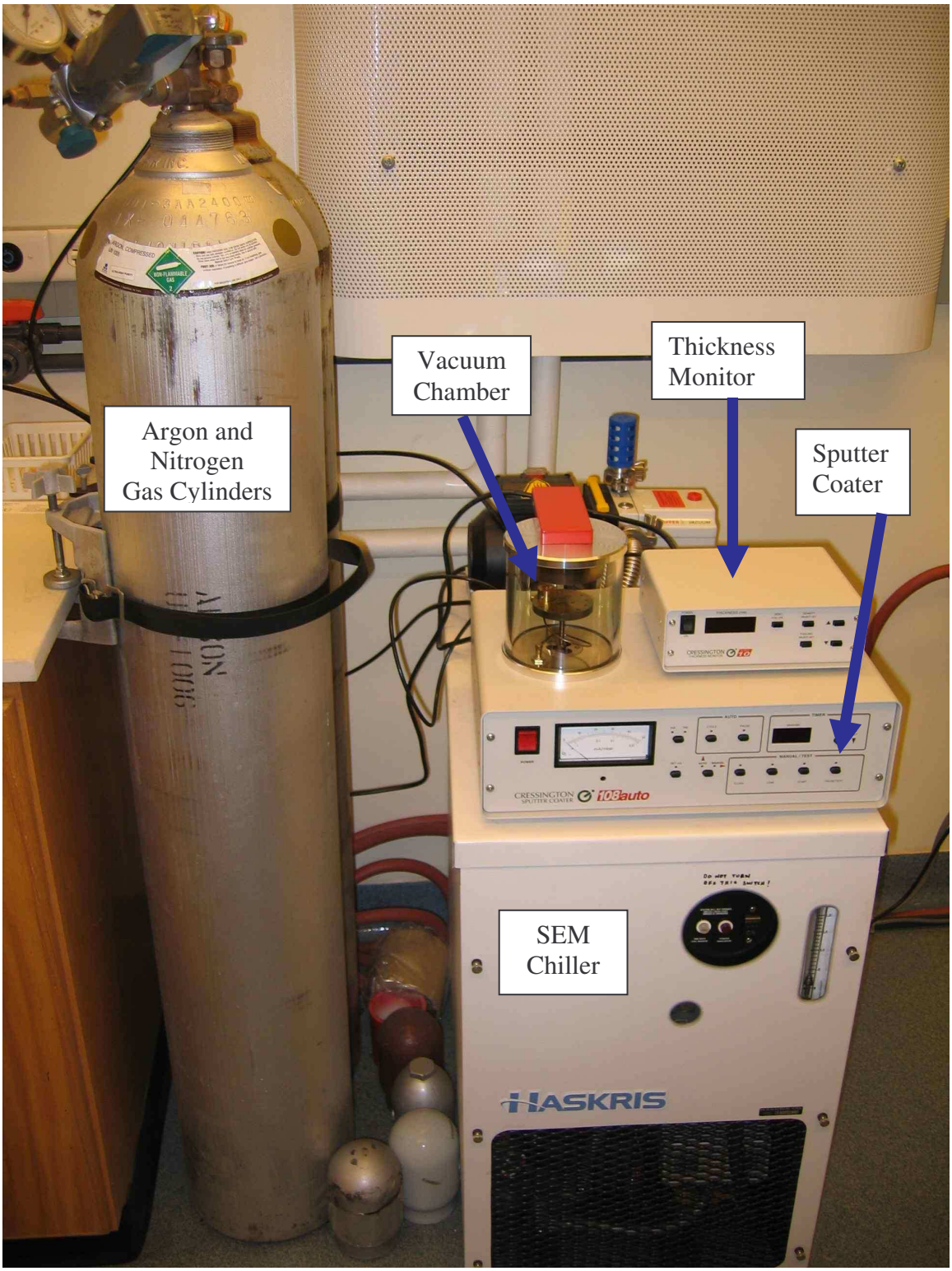

Figure 22. Sputter Coater

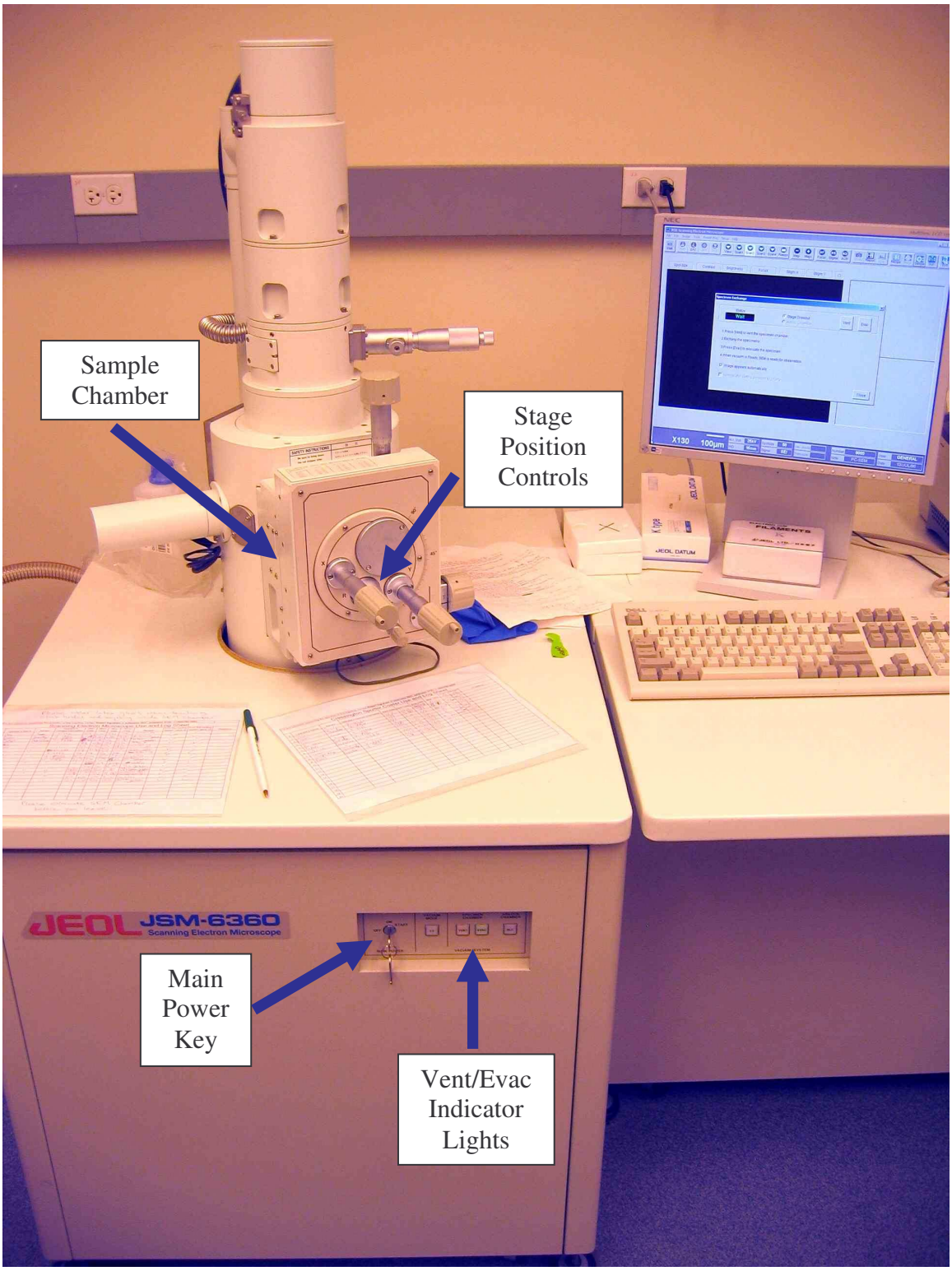

Figure 23. Scanning Electron Microscope

VITA

BENJAMIN J. LAWRENCE

Candidate for the Degree of

Master of Science

Thesis: COMPOSITE SCAFFOLDS OF NATURAL AND SYNTHETIC POLYMERS FOR BLADDER TISSUE ENGINEERING

Major Field: Chemical Engineering

Biographical:

Personal Data: Born in Tulsa, Oklahoma, on March 16, 1980, son of Larry and Sharon Lawrence

Education: Graduated from Union High School, Tulsa, Oklahoma in May 1999; received a Bachelor of Science degree in Chemical Engineering from Oklahoma State University, Stillwater, Oklahoma in May 2004; Completed the requirements for the Master of Science degree with a major in Chemical Engineering at Oklahoma State University in July 2006.

Experience: Has performed as a puppeteer, musician, juggler, and dashing rogue from high school to present; employed by Oklahoma State University (2001-2004) and the University of Colorado, Boulder (summer 2003) as an undergraduate research assistant; currently employed by the Oklahoma State University department of Chemical Engineering as a graduate research and teaching assistant.

Name: BENJAMIN J. LAWRENCE Date of Degree: July 2006

Institution: Oklahoma State University Location: Stillwater, Oklahoma

Title of Study: COMPOSITE SCAFFOLDS OF NATURAL AND SYNTHETIC POLYMERS FOR BLADDER TISSUE ENGINEERING

Pages in Study: 56 Candidate for the Degree of Master of Science

Major Field: Chemical Engineering

Scope and Method of Study: The study evaluated the formation of three layer composite tissue scaffolds using both natural and synthetic polymers. The scaffolds consisted of a perforated PLGA film sandwiched between two porous chitosan layers.

Findings and Conclusions: Composite scaffolds with a layered structure (chitosan-PLGA-chitosan) were formed through a combination of solvent casting and controlled-rate freezing and lyophilization. The 3D architecture, stress-strain behavior, and permeability to urea of these scaffolds was determined. Additionally, a four week long degradation study and a fibroblast cell culture study were performed. The results show that the composite scaffolds contain both the layered and porous structural features. The composite scaffold shows significant potential for use in tissue engineering applications. The composite contains both layered and porous structural features and provides suitable mechanical properties. The scaffold is relatively impermeable to urea. The composite demonstrates the capacity for cell colonization and the potential for cell growth.

Advisor's Approval: Dr. Sundararajan V. Madihally